

# On Bragg resonances and wave triad interactions in two-layered shear flows

Raunak Raj<sup>1</sup> and Anirban Guha<sup>1†</sup>

<sup>1</sup>Environmental and Geophysical Fluids Group, Department of Mechanical Engineering, Indian Institute of Technology, Kanpur, U.P. 208016, India.

(Received xx; revised xx; accepted xx)

The standard resonance conditions for Bragg scattering as well as weakly nonlinear wave triads have been traditionally derived in the absence of any background velocity. In this paper, we have studied how these resonance conditions get modified when uniform, as well as various piecewise linear velocity profiles, are considered. Background velocity can influence the resonance conditions in two ways (i) by causing Doppler shifts, and (ii) by changing the intrinsic frequencies of the waves. For Bragg resonance, even a uniform velocity field changes the resonance condition. Velocity shear strongly influences the resonance conditions since, in addition to changing the intrinsic frequencies, it can cause unequal Doppler shifts between the surface, pycnocline, and the bottom. Using multiple scale analysis and Fredholm alternative, we analytically obtain the equations governing both wave triads and Bragg resonances. We have also extended the Higher Order Spectral method, a highly efficient computational tool usually used to study triad and Bragg resonance problems, to incorporate the effect of piecewise linear velocity profile. A significant aspect, both in theoretical and numerical fronts, has been extending the potential flow approximation, which is the basis of studying these kinds of problems, to incorporate piecewise constant background shear.

**Key words:** Bragg resonance, stratified shear flow, flow over topography.

## 1. Introduction

‘Wave triad interaction’ – the nonlinear interaction between three waves (or modes) satisfying a certain resonant condition, is a fundamental mechanism of energy transfer in fluid flows due to the nonlinear nature of the governing Navier-Stokes equations. In a two-layered density stratified flow in the absence of background velocity, Ball (1964) showed that two counter-propagating surface gravity waves can give rise to an interfacial gravity wave by forming a wave triad. Although Ball had ruled out the possibility of the existence of any other triads involving two surface modes, such interactions were later observed between three co-propagating modes – two surface waves and one interfacial wave (Baker *et al.* 1982). In fact, two counter-propagating interfacial gravity waves can also give rise to a surface gravity wave (Wen 1995; Hill & Foda 1996). Remarkably enough, a rippled bottom topography can act like a neutral, stationary wave and mediate nonlinear energy transfer between two waves – a phenomenon known as the ‘Bragg resonance’ (Davies 1982; Mei 1985; Kirby 1986). Bragg resonance strongly affects the wave spectrum in continental shelves and coastal regions (Ball 1964), and also modifies

---

† Email address for correspondence: anirbanguha.ubc@gmail.com

the shore-parallel sandbars (Heathershaw & Davies 1985; Elgar *et al.* 2003). The study on Bragg resonance was performed in a two-layered density stratified flow by Alam *et al.* (2009a). They showed that second order nonlinearity causes a surface wave propagating over a rippled bottom to transfer energy to (i) an interfacial wave propagating in the same direction (of the surface wave), (ii) an interfacial wave propagating in the opposite direction, or (iii) a surface wave propagating in the same direction, depending on the wavenumber of the bottom ripple. Similar results were also obtained for an interfacial wave. Alam *et al.* (2009a) also studied interactions up to the third order of nonlinearity, thereby giving rise to various classes of Bragg resonance. The numerical simulations for the same were performed using a Higher Order Spectral (HOS) code (Alam *et al.* 2009b), which was initially developed for a single layered flow over bottom topography by Dommermuth & Yue (1987). Although the equations governing a single triad can also be analytically obtained without much difficulty up to the second order of nonlinearity, numerical simulation allows one to incorporate multiple triads up to several orders of nonlinearity. In most of the above-mentioned analytical and numerical (e.g. HOS) studies on wave triads or Bragg resonances, the base velocity was assumed to be absent. This is because these analytical and numerical treatments were based on the potential flow theory. The primary advantage of using the potential flow assumption is that it leads to an outstanding simplification – one can solve for the interfaces only. This allows a deeper insight into the complex nonlinear problem of resonant triad interactions and subsequent energy transfer. A general base flow falls beyond the purview of the potential flow theory, neither in such flows the dynamics remain confined at the interfaces.

Since atmospheric and oceanic flows always have base velocities (Vallis 2017), application of the ‘standard’ potential flow theory in such flows may be an over-simplification. In this work, we have considered a two-layered density stratified flow in the presence of a piecewise linear base velocity profile. We have shown that such kind of velocity profiles can be included under the umbrella of the *extended* potential flow theory. Therefore, the dynamics is still localized at the interfaces, even though there is a base velocity present. Piecewise linear base velocity implies that the base vorticity is layerwise constant. Here, no vorticity is generated in the perturbed flow. In other words, if the initial disturbances are irrotational, the perturbed flow remains irrotational forever, despite the fact that the base flow is vortical. This fundamental concept has also allowed us to use and extend the general framework of the HOS method by incorporating a piecewise linear velocity profile. In the case of wave triad interaction, adding a constant base velocity doesn’t change the dynamics of the problem and the solution is merely Doppler shifted. It can also be intuitively seen that adding a uniform flow ‘ $U$ ’ is similar to moving in a reference frame with a velocity ‘ $U$ ’, and change of the reference frame should not change the dynamics of a problem. Any non-trivial base velocity profile, however, will break the otherwise symmetric nature of the dispersion relation of surface/interfacial gravity waves. Addition of a constant base velocity leads to a significant alteration in the resonance conditions for Bragg resonance (Kirby 1988); here the Doppler shift is not simply equivalent to changing of the reference frame because of the involvement of the bottom topography. The fact that the bottom topography is at rest while the surface and the interface have some base flow results in unequal Doppler shift between the surface/interface and the bottom topography.

Significant changes occur when a uniform shear is present in each layer. When there is a jump in the base vorticity (i.e. shear) across an interface, it leads to vorticity waves. In addition, if there is a buoyancy jump at the same interface, we get vorticity-gravity waves (Harnik *et al.* 2008). Interaction between an interfacial vorticity wave (with no buoyancy jump) and a surface gravity wave was the focus of a recent study by Drivas & Wunsch

(2016). Due to the presence of shear, the surface and the interface move with different base velocities, which significantly alters the conditions for the formation of resonant triads. Therefore, we expect that the problems involving triad interactions and Bragg resonances are remarkably enriched when piecewise linear base velocity field is present.

The paper is organized as follows. In §2, we have shown the applicability of potential flow theory to a piecewise linear velocity profiles. Furthermore, we have derived the modified evolution equations, which has been subsequently applied to the HOS Code in order to incorporate the velocity field. We also use the evolution equations to obtain the dispersion relation of a general two-layered flow with a velocity field. This is followed by a perturbation expansion of the variables till  $\mathcal{O}(\epsilon^2)$ , and using the Fredholm's alternative, we obtain the analytical solution for amplitude variation both for the case of Bragg resonance and wave triad interaction. In §3, we have explored the effect of different types of velocity fields on different types of Bragg resonance triads using dispersion relations. In §4, we have briefly explained the effect of velocity field on wave triad interactions. We have devoted the §5 to the numerical code and simulation. In this section, we have described the HOS code, which we have extended to incorporate piecewise linear velocity profiles. After validating the code, we have shown some numerical simulations to corroborate our analytical derivations. Finally, we summarize and conclude the paper in §6.

## 2. Theory

The kinematic boundary conditions and the dynamic boundary conditions for the water wave problem are nonlinear, suggesting that waves can interchange energy between them through a nonlinear interaction. This nonlinear exchange of energy between the waves, known as the wave triad interaction, is maximum when the waves involved satisfy a specific resonance condition. Although the energy exchange is a weakly nonlinear phenomenon, the condition for triad interactions can simply be obtained from the linear dispersion relations. The condition for the resonance between waves of wavenumbers  $(k_1, k_2$  and  $k_3)$  and frequencies  $(\omega_1, \omega_2$  and  $\omega_3)$  is

$$k_3 = k_1 \pm k_2, \quad (2.1a)$$

$$\omega_3 = \omega_1 \pm \omega_2. \quad (2.1b)$$

The above condition basically means that if on the  $k$ - $\omega$  plane, waves are denoted by the vectors  $(k_1, \omega_1)$ ,  $(k_2, \omega_2)$  and  $(k_3, \omega_3)$ , then these vectors are linearly dependent (Ball 1964). Further, when two waves exchange energy with each other via mediation of the bottom ripples, which acts as a stationary wave with zero frequency, it is known as the Bragg resonance. Here, the resonance condition becomes

$$k_2 = k_1 \pm k_b, \quad (2.2a)$$

$$\omega_1 = \omega_2. \quad (2.2b)$$

For the case of no velocity, the dispersion relation is a biquadratic polynomial in  $\omega$ , and is given as (Ball 1964; Alam *et al.* 2009a)

$$\omega^4(R + \coth kh_u \coth kh_l) - \omega^2 gk(\coth kh_u + \coth kh_l) + g^2 k^2(1 - R) = 0. \quad (2.3)$$

Here  $R \equiv \rho_u/\rho_l$  is the density ratio, and  $h_u$  and  $h_l$  are respectively the depths of the upper and lower layers. Throughout the paper, the subscripts  $u$  and  $l$  respectively denote 'upper' and 'lower'. The implication of (2.3) being a biquadratic in  $\omega$  is that the leftward travelling waves and the rightward travelling waves are symmetric, i.e. the

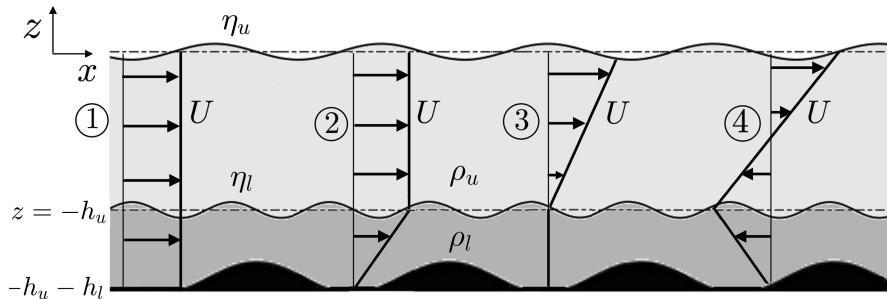


Figure 1: Schematic of a two-layered density stratified flow in presence of bottom topography and various kinds of simple velocity shear, labelled by ① (uniform flow), ② (constant shear in the bottom layer), ③ (constant shear in the top layer), and ④ (constant shear in both layers).

difference between the two is simply a matter of a change in the sign of  $\omega$ . However, in the presence of a uniform velocity  $U$ , the intrinsic frequencies of the waves are Doppler shifted by an amount ' $Uk$ '. Further, if the velocity field is a function of the vertical coordinate ' $z$ ', then there can be a presence of a vorticity wave also, which will alter the intrinsic frequency of the waves as well, and the biquadratic and symmetric nature of the dispersion relation will be lost. We have classified the velocity profiles into 4 categories: (i) a uniform flow (ii) shear only in the lower layer (iii) shear only in the upper layer (iv) shear in both the layers. These cases have been shown in the figure 1. In the first case, the surface and the interface are not Doppler shifted with respect to each other but they are Doppler shifted with respect to the bottom. This should mean that the condition for wave triad interaction will not change but the condition for Bragg resonance should get altered. Further, there won't be any change in the intrinsic frequencies of any of the waves present in the system. In the second case, shear is only present in the lower layer. This case is similar to the first one with reference to the Doppler shifts, i.e. both the surface, and the interface between  $\rho_u$  and  $\rho_l$  (hereafter, simply referred to as 'interface' or 'pycnocline'), are Doppler shifted equally with respect to the bottom, but additionally, the intrinsic frequencies of waves will change due to the presence of a shear jump at the interface. In the third case, shear is present only in the upper layer and hence the surface and the interface are Doppler shifted; moreover, there is a presence of a shear jump at the interface too. Hence, the intrinsic frequencies of the waves will also change. In the last case, shear is present in both layers. Hence, there is a shear jump both at the interface and at the surface and the surface and the interface are Doppler shifted unequally with respect to the bottom. It is also to be noted here that the velocity difference between the surface and the interface, i.e. the second and the fourth cases might lead to linear instabilities as well due to the formation of counter-propagating system (Guha & Lawrence 2014). However, such linear instabilities, for moderate values of shear are restricted to high wavenumbers and don't have appreciable growth rates. In any case, we would be focussing on the nonlinear interactions only.

It was shown in Guha & Raj (2017) that in the presence of a piecewise linear velocity profile, there is no perturbation vorticity generation. This means that if the flow is initially irrotational, then it will remain so forever, similar to the scenario of no background velocity. Further, if there is a density difference ( $\rho_1, \rho_2$ ) as well a shear difference ( $\Omega_1, \Omega_2$ ) across any *general* (hence subscripts '1' and '2' are used, instead of 'u' and 'l') interface



$z = \eta(x, t)$  moving with a velocity  $U$ , then the dynamic boundary condition at any interface  $z = \eta(x, t)$  is given by (See Appendix A for derivation)

$$\rho_1 \left[ \phi_{1,t} + \frac{1}{2} (\phi_{1,x}^2 + \phi_{1,z}^2) + U\phi_{1,x} - \Omega_1\psi_1 + g\eta \right] = \rho_2 \left[ \phi_{2,t} + \frac{1}{2} (\phi_{2,x}^2 + \phi_{2,z}^2) + U\phi_{2,x} - \Omega_2\psi_2 + g\eta \right]. \quad (2.4)$$

Here,  $\phi_1$  and  $\phi_2$  are respectively the perturbation velocity potentials of fluids ‘1’ and ‘2’, while  $\psi_1$  and  $\psi_2$  are the same for the streamfunctions, which can be obtained using the respective velocity potentials. The comma in the subscript denotes partial derivative; for example,  $\eta_{1,x} \equiv \partial\eta_1/\partial x$ . In the above equation, the terms  $U\phi_{1,x}$  and  $U\phi_{2,x}$  are the ‘Doppler shift’ terms indicating that the interface is moving at a velocity  $U$ . The terms  $\Omega_1\psi_1$  and  $\Omega_2\psi_2$  appear due to the presence of the constant shears  $\Omega_1$  and  $\Omega_2$  on either side of the interface. Rest all other terms are usual and appear in the absence of velocity as well. Similarly, the kinematic boundary condition for the same interface will be given by

$$\eta_{,t} + (U + \phi_{,x})\eta_{,x} = \phi_{,z}. \quad (2.5)$$

Here, the term  $U\eta_{,x}$  is the Doppler shift term. Unlike the dynamic boundary condition, the kinematic boundary condition doesn’t depend on the shear on the either side of the interface. We will apply both kinematic and dynamic boundary conditions to the surface and the interface in figure 1.

## 2.1. Framework

Here we give a general framework that consists of a system of equations at  $\mathcal{O}(\epsilon)$  and  $\mathcal{O}(\epsilon^2)$ , which is obtained using perturbation analysis and the method of multiple scales for a periodic wave train. We have kept the system quite general so as to use the system of equations for the purpose of wave triad interaction (see §2.2) and Bragg resonance (see §2.3).

We consider a two-interface system with piecewise constant density and vorticity in each layer, see figure 1. The velocity profile is continuous, but the derivative of velocity may have a discontinuity at the density interface. Total depth of the system is  $H$  and  $H = h_u + h_l$ . The fluid above the surface is assumed to be a zero density fluid and  $R$  is the density ratio at the interface ( $R \equiv \rho_u/\rho_l$ ). The base velocity profile is piecewise linear, and has the values  $U = \{U_u, U_l, U_b\}$  at  $z = \{0, -h_u, -h_u - h_l\}$  respectively. The vertical ( $z$ ) axis points upwards, hence the gravity ( $g$ ) is along the negative  $z$ -direction. The elevations of the surface and the pycnocline from their respective mean level are  $\eta_u(x, t)$  and  $\eta_l(x, t)$ . Similarly, the elevation of the bottom topography is  $\eta_b(x)$  from its mean level at  $z = -h_u - h_l$ . For initial irrotational disturbances and for piecewise linear velocity profile, it was shown in Guha & Raj (2017) that the vorticity generation is limited to the interfaces and the bulk flow remains irrotational. This allows us to introduce the velocity potentials  $\phi_u$  and  $\phi_l$  respectively in the upper and the lower layers. Hence, the continuity equation reduces to the Laplace equation

$$\nabla^2\phi_u = 0 \quad -h_u + \eta_l < z < \eta_u, \quad (2.6a)$$

$$\nabla^2\phi_l = 0 \quad -h_u - h_l + \eta_b < z < -h_u + \eta_l. \quad (2.6b)$$

The kinematic boundary conditions are

$$\eta_{u,t} + (U_u + \phi_{u,x})\eta_{u,x} = \phi_{u,z} \quad \text{at } z = \eta_u, \quad (2.7a)$$

$$\eta_{l,t} + (U_l + \phi_{u,x})\eta_{l,x} = \phi_{u,z} \quad \text{at } z = -h_u + \eta_l, \quad (2.7b)$$

$$\eta_{l,t} + (U_l + \phi_{l,x})\eta_{l,x} = \phi_{l,z} \quad \text{at } z = -h_u + \eta_l, \quad (2.7c)$$

$$(U_b + \phi_{l,x})\eta_{b,x} = \phi_{l,z} \quad \text{at } z = -h_u - h_l + \eta_b. \quad (2.7d)$$

Likewise, the dynamic boundary conditions are as follows:

$$\phi_{u,t} + \frac{1}{2} (\phi_{u,x}^2 + \phi_{u,z}^2) + U_u \phi_{u,x} - \Omega_u \psi_u + g\eta_u = 0 \quad \text{at } z = \eta_u, \quad (2.7e)$$

$$\rho_u \left[ \phi_{u,t} + \frac{1}{2} (\phi_{u,x}^2 + \phi_{u,z}^2) + U_l \phi_{u,x} - \Omega_u \psi_u + g\eta_l \right] \\ - \rho_l \left[ \phi_{l,t} + \frac{1}{2} (\phi_{l,x}^2 + \phi_{l,z}^2) + U_l \phi_{l,x} - \Omega_l \psi_l + g\eta_l \right] = 0 \quad \text{at } z = -h_u + \eta_l. \quad (2.7f)$$

We are interested in obtaining the solutions up to a  $\mathcal{O}(\epsilon^2)$  and hence, using a perturbation expansion, we get

$$\phi_u(x, z, t) = \epsilon \phi_u^{(1)}(x, z, t, \tau) + \epsilon^2 \phi_u^{(2)}(x, z, t, \tau), \quad (2.8a)$$

$$\phi_l(x, z, t) = \epsilon \phi_l^{(1)}(x, z, t, \tau) + \epsilon^2 \phi_l^{(2)}(x, z, t, \tau), \quad (2.8b)$$

$$\eta_u(x, t) = \epsilon \eta_u^{(1)}(x, t, \tau) + \epsilon^2 \eta_u^{(2)}(x, t, \tau), \quad (2.8c)$$

$$\eta_l(x, t) = \epsilon \eta_l^{(1)}(x, t, \tau) + \epsilon^2 \eta_l^{(2)}(x, t, \tau). \quad (2.8d)$$

Here we have assumed that the potentials and elevations have a slow time scale ‘ $\tau$ ’ associated with them such that  $\tau = \epsilon t$ . The superscripts (1) and (2) respectively denote the  $\mathcal{O}(\epsilon)$  and  $\mathcal{O}(\epsilon^2)$  terms. Further, we expand the velocity potential  $\phi$  and the streamfunction  $\psi$  in a Taylor series about the respective mean surface/interface, which at  $\mathcal{O}(\epsilon)$  gives the following set of equations:

$$\phi_{u,z}^{(1)} - \eta_{u,t}^{(1)} - U_u \eta_{u,x}^{(1)} = 0 \quad \text{at } z = 0, \quad (2.9a)$$

$$\phi_{u,z}^{(1)} - \eta_{l,t}^{(1)} - U_l \eta_{l,x}^{(1)} = 0 \quad \text{at } z = -h_u, \quad (2.9b)$$

$$\phi_{l,z}^{(1)} - \eta_{l,t}^{(1)} - U_l \eta_{l,x}^{(1)} = 0 \quad \text{at } z = -h_u, \quad (2.9c)$$

$$\phi_{u,t}^{(1)} + U_u \phi_{u,x}^{(1)} - \Omega_u \psi_u^{(1)} + g\eta_u^{(1)} = 0 \quad \text{at } z = 0, \quad (2.9d)$$

$$R \left[ \phi_{u,t}^{(1)} + U_l \phi_{u,x}^{(1)} - \Omega_u \psi_u^{(1)} + g\eta_l^{(1)} \right] \quad (2.9e)$$

$$- \left[ \phi_{l,t}^{(1)} + U_l \phi_{l,x}^{(1)} - \Omega_l \psi_l^{(1)} + g\eta_l^{(1)} \right] = 0 \quad \text{at } z = -h_u, \quad (2.9f)$$

$$\phi_{l,z}^{(1)} = 0 \quad \text{at } z = -h_u - h_l \quad (2.9g)$$

Additionally, we use the eigenfunction expansions with slowly varying amplitudes satisfying the respective Laplace equations. Thus for  $j = \{1, 2, \dots\}$  and  $m = \{1, 2\}$ , where the subscript  $j$  denotes the  $j$ -th wavenumber and the superscript ( $m$ ) denotes the order of

nonlinearity, we get

$$\phi_{uj}^{(m)} = \left[ A_j^{(m)}(\tau) \frac{\cosh k_j(z + h_u)}{\cosh(k_j h_u)} + B_j^{(m)}(\tau) \frac{\sinh k_j(h_u)}{\cosh(k_j h_u)} \right] e^{i(k_j x - \omega_j t)} + \text{c.c.}, \quad (2.10a)$$

$$\phi_{lj}^{(m)} = \left[ C_j^{(m)}(\tau) \frac{\cosh k_j(z + h_u + h_l)}{\cosh(k_j h_l)} + D_j^{(m)}(\tau) \frac{\sinh k_j(z + h_u + h_l)}{\cosh(k_j h_l)} \right] e^{i(k_j x - \omega_j t)} + \text{c.c.}, \quad (2.10b)$$

$$\psi_{uj}^{(m)} = i \left[ A_j^{(m)}(\tau) \frac{\sinh k_j(z + h_u)}{\cosh(k_j h_u)} + B_j^{(m)}(\tau) \frac{\cosh k_j(h_u)}{\cosh(k_j h_u)} \right] e^{i(k_j x - \omega_j t)} + \text{c.c.}, \quad (2.10c)$$

$$\psi_{lj}^{(m)} = i \left[ C_j^{(m)}(\tau) \frac{\sinh k_j(z + h_u + h_l)}{\cosh(k_j h_l)} + D_j^{(m)}(\tau) \frac{\cosh k_j(z + h_u + h_l)}{\cosh(k_j h_l)} \right] e^{i(k_j x - \omega_j t)} + \text{c.c.}, \quad (2.10d)$$

$$\eta_{uj}^{(m)} = a_j^{(m)}(\tau) e^{i(k_j x - \omega_j t)} + \text{c.c.}, \quad (2.10e)$$

$$\eta_{lj}^{(m)} = b_j^{(m)}(\tau) e^{i(k_j x - \omega_j t)} + \text{c.c.}, \quad (2.10f)$$

where c.c. denotes complex conjugate. Substituting the above equations (2.10a)–(2.10f) in the equations (2.9a)–(2.9g) at  $\mathcal{O}(\epsilon)$ , we obtain a set of linear equations corresponding to any given wavenumber  $k_j$  at  $\mathcal{O}(\epsilon)$

$$\underline{\underline{\mathfrak{D}}}(\omega_j, k_j) \mathbf{x}_j^{(1)} = 0. \quad (2.11)$$

Here, the vector  $\mathbf{x}_j^{(1)} \equiv [A_j^{(1)}, B_j^{(1)}, C_j^{(1)}, D_j^{(1)}, a_j^{(1)}, b_j^{(1)}]^\dagger$ , and the matrix  $\underline{\underline{\mathfrak{D}}}(\omega_j, k_j)$  is given by

$$\begin{bmatrix} \frac{k_j}{\coth(k_j h_u)} & \frac{k_j}{\cosh(k_j h_u)} & 0 & 0 & i\omega_j^{\{1\}} & 0 \\ 0 & k_j & 0 & 0 & 0 & i\omega_j^{\{2\}} \\ 0 & 0 & \frac{k_j}{\coth(k_j h_l)} & k & 0 & i\omega_j^{\{2\}} \\ -i\omega_j^{\{1\}} - \frac{i\Omega_u}{\coth(k_j h_u)} & -\frac{i\Omega_u}{\cosh(k_j h_u)} & 0 & 0 & g & 0 \\ -\frac{iR\omega_j^{\{2\}}}{\cosh(k_j h_u)} & \frac{iR\omega_j^{\{2\}}}{\coth(k_j h_u)} - iR\Omega_u & i\omega_j^{\{2\}} + \frac{i\Omega_l}{\coth k_j h_l} & \frac{i\omega_j^{\{2\}}}{\coth k_j h_l} + i\Omega_l & 0 & g(R-1) \\ 0 & 0 & 0 & \frac{k_j}{\cosh k_j h_l} & 0 & 0 \end{bmatrix}$$

where  $\omega_j^{\{1\}} = \omega_j - U_u k_j$  ;  $\omega_j^{\{2\}} = \omega_j - U_l k_j$ . The dispersion relation of the above system is obtained by setting the determinant of the above matrix to zero and is given by the equation

$$\mathfrak{D}(\omega_j, k_j) = 0, \quad (2.12)$$

where  $\mathfrak{D}(\omega_j, k_j)$  is the determinant of the matrix  $\underline{\underline{\mathfrak{D}}}(\omega_j, k_j)$ . At  $\mathcal{O}(\epsilon^2)$ , we obtain the

following equations:

$$\phi_{u,z}^{(2)} - \eta_{u,t}^{(2)} - U_u \eta_{u,x}^{(2)} = p_1 + q_1 \quad \text{at } z = 0, \quad (2.13a)$$

$$\phi_{u,z}^{(2)} - \eta_{l,t}^{(2)} - U_l \eta_{l,x}^{(2)} = p_2 + q_2 \quad \text{at } z = -h_u, \quad (2.13b)$$

$$\phi_{l,z}^{(2)} - \eta_{l,t}^{(2)} - U_l \eta_{l,x}^{(2)} = p_3 + q_3 \quad \text{at } z = -h_u, \quad (2.13c)$$

$$\phi_{u,t}^{(2)} + U_u \phi_{u,x}^{(2)} - \Omega_u \psi_u^{(2)} + g \eta_u^{(2)} = p_4 + q_4 \quad \text{at } z = 0, \quad (2.13d)$$

$$\begin{aligned} & \left[ \phi_{u,t}^{(2)} + U_l \phi_{u,x}^{(2)} - \Omega_u \psi_u^{(2)} + g \eta_l^{(2)} \right] \\ & - \left[ \phi_{l,t}^{(2)} + U_l \phi_{l,x}^{(2)} - \Omega_l \psi_l^{(2)} + g \eta_l^{(2)} \right] = p_5 + q_5 \quad \text{at } z = -h_u, \end{aligned} \quad (2.13e)$$

$$\phi_{l,z}^{(2)} = p_6 + q_6 \quad \text{at } z = -h_u - h_l. \quad (2.13f)$$

The RHS terms  $p_1, p_2, p_3, p_4, p_5$  and  $p_6$  are the products of two  $\mathcal{O}(\epsilon)$  terms and are given as

$$p_1 = \eta_{u,x} \phi_{u,x} - \eta_u \phi_{u,zz} \quad z = 0, \quad (2.14a)$$

$$p_2 = \eta_{l,x} \phi_{u,x} - \eta_l \phi_{u,zz} \quad z = -h_u, \quad (2.14b)$$

$$p_3 = \eta_{l,x} \phi_{l,x} - \eta_l \phi_{l,zz} \quad z = -h_u, \quad (2.14c)$$

$$p_4 = -\eta_u (\phi_{u,tz} - U_u \phi_{u,xz}) - \frac{1}{2} [(\phi_{u,x})^2 + (\phi_{u,z})^2] + \Omega_u \eta_u \psi_{u,z} \quad z = 0, \quad (2.14d)$$

$$\begin{aligned} p_5 = R & \left[ \eta_l (\phi_{u,tz} - U_l \phi_{u,xz}) - \frac{1}{2} [(\phi_{u,x})^2 + (\phi_{u,z})^2] + \Omega_u \eta_l \psi_{u,z} \right] \\ & - \left[ \eta_l (\phi_{l,tz} - U_l \phi_{l,xz}) - \frac{1}{2} [(\phi_{l,x})^2 + (\phi_{l,z})^2] + \Omega_l \eta_l \psi_{l,z} \right] \quad z = -h_u, \end{aligned} \quad (2.14e)$$

$$p_6 = \eta_{b,x} \phi_{l,x} - \eta_b \phi_{l,zz} \quad z = -h_u - h_l. \quad (2.14f)$$

The RHS terms  $q_1, q_2, q_3, q_4, q_5$  and  $q_6$  are the time derivatives of the  $\mathcal{O}(\epsilon)$  terms:

$$q_1 = \eta_{u,\tau}, \quad (2.15a)$$

$$q_2 = \eta_{l,\tau}, \quad (2.15b)$$

$$q_3 = \eta_{l,\tau}, \quad (2.15c)$$

$$q_4 = -\dot{\phi}_{u,\tau}, \quad (2.15d)$$

$$q_5 = -R \dot{\phi}_{u,\tau} + \dot{\phi}_{l,\tau}, \quad (2.15e)$$

$$q_6 = 0. \quad (2.15f)$$

The set of equations obtained till here are very general and works both for the case of wave triad interaction and Bragg resonance. This is because till here, we haven't made any assumption on the wavenumbers present in the system or if those wavenumbers satisfy any particular resonance condition. Hence, we will be using the above framework to obtain the analytical solutions for wave triad interaction in §2.2 as well as Bragg resonance in §2.3.

## 2.2. Analytical solution for wave triad interaction

We assume that initially at  $\mathcal{O}(\epsilon)$ , the system has only 3 wavenumbers  $\{k_1, k_2, k_3\}$  and corresponding frequencies  $\{\omega_1, \omega_2, \omega_3\}$ , satisfying the resonance condition. Without any loss of generality, the resonance condition is given by  $k_1 = k_2 + k_3$  and  $\omega_1 = \omega_2 + \omega_3$ .

The surface elevation expressed as a sum of these three modes read

$$\eta_u^{(1)}(x, t, \tau) = a_1^{(1)}(\tau)e^{i(k_1x - \omega_1t)} + a_2^{(1)}(\tau)e^{i(k_2x - \omega_2t)} + a_3^{(1)}(\tau)e^{i(k_3x - \omega_3t)} + c.c. \quad (2.16)$$

The other functions  $\phi_u^{(1)}, \phi_l^{(1)}, \psi_u^{(1)}, \psi_l^{(1)}, \psi_i^{(1)}$  and  $\eta_l^{(1)}$  can also be written in a similar fashion. Substituting this in the equations at  $\mathcal{O}(\epsilon)$ , we would obtain the following set of linear equations:

$$\underline{\underline{\mathfrak{D}}}(\omega_1, k_1)\mathbf{x}_1^{(1)} = 0 \quad ; \quad \underline{\underline{\mathfrak{D}}}(\omega_2, k_2)\mathbf{x}_2^{(1)} = 0 \quad ; \quad \underline{\underline{\mathfrak{D}}}(\omega_3, k_3)\mathbf{x}_3^{(1)} = 0. \quad (2.17)$$

The vector  $\mathbf{x}_j^{(1)} \equiv [A_j^{(1)}, B_j^{(1)}, C_j^{(1)}, D_j^{(1)}, a_j^{(1)}, b_j^{(1)}]^\dagger$  and the matrix  $\underline{\underline{\mathfrak{D}}}(\omega, k)$  are given in §2.1. We further proceed to substitute (2.10a)–(2.10f) in (2.13a)–(2.13f) at  $\mathcal{O}(\epsilon^2)$ . Here, the LHS of the equations obtained at  $\mathcal{O}(\epsilon^2)$  is similar to those obtained at  $\mathcal{O}(\epsilon)$ . On substitution, we collect the terms corresponding to each wavenumber  $k_1, k_2$  and  $k_3$  after using the resonance condition  $k_1 = k_2 + k_3$  and  $\omega_1 = \omega_2 + \omega_3$ . We obtain equations of the form

$$\underline{\underline{\mathfrak{D}}}(\omega_1, k_1)\mathbf{x}_1^{(2)} = \mathbf{v}_1 a_2^{(1)} a_3^{(1)} + \mathbf{r}_1 a_{1,\tau}^{(1)}, \quad (2.18a)$$

$$\underline{\underline{\mathfrak{D}}}(\omega_2, k_2)\mathbf{x}_2^{(2)} = \mathbf{v}_2 \bar{a}_3^{(1)} a_1^{(1)} + \mathbf{r}_2 a_{2,\tau}^{(1)}, \quad (2.18b)$$

$$\underline{\underline{\mathfrak{D}}}(\omega_3, k_3)\mathbf{x}_3^{(2)} = \mathbf{v}_3 a_1^{(1)} \bar{a}_2^{(1)} + \mathbf{r}_3 a_{3,\tau}^{(1)}, \quad (2.18c)$$

where overbar denotes complex conjugate. The vector  $\mathbf{x}_j^{(2)} \equiv [A_j^{(2)}, B_j^{(2)}, C_j^{(2)}, D_j^{(2)}, a_j^{(2)}, b_j^{(2)}]^\dagger$  and the terms of the vector  $\mathbf{v}_j$  and  $\mathbf{r}_j$  are given in the appendix A. The vector  $\mathbf{v}_j$  comes from the coefficient of  $\exp[i(k_jx - \omega_jt)]$  present in the product of two  $\mathcal{O}(\epsilon)$  terms. Similarly, the vector  $\mathbf{r}$  comes from the time derivatives of  $\mathcal{O}(\epsilon)$  terms. It might be noted here that the product terms contain combinations of various terms such as  $A_i^{(1)} a_j^{(1)}, B_i^{(1)} a_j^{(1)}, C_i^{(1)} C_j^{(1)}$  etc; however, we have converted each of these products into the product  $a_i^{(1)} a_j^{(1)}$ , i.e. in terms of products of amplitude of surface elevation by using the null space of the respective matrix  $\underline{\underline{\mathfrak{D}}}(\omega, k)$ . Similarly, the slow time derivatives are also converted in terms of the slow time derivative of the surface elevations, i.e.  $a_{j,\tau}^{(1)}$ .

Using the Fredholm alternative in the context of the sets of equations (2.17) and (2.18), we deduce that the solutions for  $\mathbf{x}_i^{(2)}$  exist if and only if the vectors  $\mathbf{v}_i$  are orthogonal to the null space of the transpose of the respective matrices  $\underline{\underline{\mathfrak{D}}}(\omega_j, k_j)$ . Denoting the null space of the transpose of matrix  $\underline{\underline{\mathfrak{D}}}(\omega_j, k_j)$  by  $\mathbf{n}_j$ , we finally get a set of three equations:

$$\mathbf{n}_1 \cdot \left( \mathbf{v}_1 a_2^{(1)} a_3^{(1)} + \mathbf{r}_1 a_{1,\tau}^{(1)} \right) = 0, \quad (2.19a)$$

$$\mathbf{n}_2 \cdot \left( \mathbf{v}_2 \bar{a}_3^{(1)} a_1^{(1)} + \mathbf{r}_2 a_{2,\tau}^{(1)} \right) = 0, \quad (2.19b)$$

$$\mathbf{n}_3 \cdot \left( \mathbf{v}_3 a_1^{(1)} \bar{a}_2^{(1)} + \mathbf{r}_3 a_{3,\tau}^{(1)} \right) = 0, \quad (2.19c)$$

which finally gets reduced to

$$a_{1,\tau}^{(1)} = \beta_1 a_2^{(1)} a_3^{(1)} \quad ; \quad a_{2,\tau}^{(1)} = \beta_2 \bar{a}_3^{(1)} a_1^{(1)} \quad ; \quad a_{3,\tau}^{(1)} = \beta_3 a_1^{(1)} \bar{a}_2^{(1)}, \quad (2.20)$$

where

$$\beta_j = -\frac{\mathbf{n}_j \cdot \mathbf{v}_j}{\mathbf{n}_j \cdot \mathbf{r}_j}. \quad (2.21)$$

### 2.3. Analytical Solution for Bragg resonance

The equations for the case of Bragg resonance can also be obtained using the same framework as in §2.2. However, in the case of Bragg resonance, only two propagating waves are involved, the third one is the bottom ripple. We assume that the participating waves have the wavenumbers  $\{k_1, k_2\}$  with frequencies  $\{\omega_1, \omega_2\}$  and the bottom with the wavenumber  $k_b$ . Substituting the normal modes, we would get a set of linear equations at  $\mathcal{O}(\epsilon)$ :

$$\underline{\underline{\mathfrak{D}}}(\omega_1, k_1)\mathbf{x}_1^{(1)} = 0 \quad ; \quad \underline{\underline{\mathfrak{D}}}(\omega_2, k_2)\mathbf{x}_2^{(1)} = 0. \quad (2.22)$$

Here the vector  $\mathbf{x}_j^{(1)} \equiv [A_j^{(1)}, B_j^{(1)}, C_j^{(1)}, D_j^{(1)}, a_j^{(1)}, b_j^{(1)}]^\dagger$  and the matrix  $\underline{\underline{\mathfrak{D}}}(\omega, k)$  are the same as that in §2.2. We assume that at  $\mathcal{O}(\epsilon)$ , the surface consists of only two modes,  $k_1$  and  $k_2$ . Hence we write  $\eta_u^{(1)}(x, t)$  as

$$\eta_u^{(1)}(x, t, \tau) = a_1^{(1)}(\tau)e^{i(k_1x - \omega_1t)} + a_2^{(1)}(\tau)e^{i(k_2x - \omega_2t)} + \text{c.c.}, \quad (2.23)$$

$$\eta_b(x) = a_b e^{ik_1x} + \text{c.c.} \quad (2.24)$$

The other functions  $\phi_u^{(1)}, \phi_l^{(1)}, \psi_u^{(1)}, \psi_l^{(1)}$  and  $\eta_l^{(1)}$  containing the wavenumbers ' $k_1$ ' and ' $k_2$ ' can also be written similarly. Substituting this in the equations at  $\mathcal{O}(\epsilon)$ , we would obtain a set of linear equations

$$\underline{\underline{\mathfrak{D}}}(\omega_1, k_1)\mathbf{x}_1^{(1)} = 0 \quad ; \quad \underline{\underline{\mathfrak{D}}}(\omega_2, k_2)\mathbf{x}_2^{(1)} = 0. \quad (2.25)$$

The vector  $\mathbf{x}_j^{(1)} \equiv [A_j^{(1)}, B_j^{(1)}, C_j^{(1)}, D_j^{(1)}, a_j^{(1)}, b_j^{(1)}]^\dagger$  and the matrix  $\underline{\underline{\mathfrak{D}}}(\omega, k)$  are the same as that in §2.2. We further proceed to substitute the equations (2.10a)–(2.10f) in the equations (2.13a)–(2.13f) at  $\mathcal{O}(\epsilon^2)$ . Assuming  $k_1 + k_2 = k_b$  and  $\omega_1 + \omega_2 = 0$ , we obtain

$$\underline{\underline{\mathfrak{D}}}(\omega_1, k_1)\mathbf{x}_1^{(2)} = \mathbf{v}_1 a_b \bar{a}_2^{(1)} + \mathbf{r}_1 a_{1,\tau}^{(1)}, \quad (2.26)$$

$$\underline{\underline{\mathfrak{D}}}(\omega_2, k_2)\mathbf{x}_2^{(2)} = \mathbf{v}_2 a_b \bar{a}_1^{(1)} + \mathbf{r}_2 a_{2,\tau}^{(1)}. \quad (2.27)$$

Denoting the null space of  $\underline{\underline{\mathfrak{D}}}(k_j, \omega_j)$  by  $\mathbf{n}_j$  and using the Fredholm alternative, we get the following set of equations:

$$a_{1,\tau}^{(1)} = \beta_1 a_b \bar{a}_2^{(1)} \quad ; \quad a_{2,\tau}^{(1)} = \beta_2 a_b \bar{a}_1^{(1)}, \quad (2.28)$$

where

$$\beta_j = -\frac{\mathbf{n}_j \cdot \mathbf{v}_j}{\mathbf{n}_j \cdot \mathbf{r}_j}. \quad (2.29)$$

Furthermore, when  $k_1 - k_2 = k_b$  and  $\omega_1 - \omega_2 = 0$ , we get

$$a_{1,\tau}^{(1)} = \beta_1 a_b a_2^{(1)} \quad ; \quad a_{2,\tau}^{(1)} = \beta_2 \bar{a}_b a_1^{(1)}, \quad (2.30)$$

in which  $\beta_j$  remains the same as before.

### 3. Bragg resonance in the presence of a velocity field

In a single layered flow in the absence of a velocity field, there can be only one condition for Bragg resonance – when the wavenumber of the bottom is twice the wavenumber of the surface wave, i.e.  $k_b = 2k_s$ . In such a case, an oppositely travelling surface mode having the same frequency as that of the incident wave is generated by the resonant forcing of the bottom. However, in a two-layered flow, several other resonant pairs are possible (Alam *et al.* 2009a). As mentioned previously, in the presence of a pycnocline,

there exists four different modes of propagation – two oppositely travelling surface (or external) modes and two oppositely travelling interfacial (or internal) modes. Any of these modes, depending on the wavenumber of the bottom ripples, may resonate with any other mode in the system, subject to the fulfilment of the resonance conditions. In the absence of velocity field, there is an inherent symmetry in the weakly nonlinear wave interaction owing to the symmetric (or biquadratic) nature of the dispersion relation. This means that if a rightward travelling surface mode of wavenumber  $k_i$  interacts with the bottom of wavenumber  $k_b$  to resonantly generate a leftward travelling interfacial mode of wavenumber  $k_r$ , then a leftward travelling surface mode of wavenumber  $k_i$  will also interact with the same bottom of wavenumber  $k_b$  to resonantly generate a rightward travelling interfacial mode of wavenumber  $k_r$ . In the presence of a velocity field, however, this ‘right-left symmetry’ of the interaction is destroyed.

The presence of velocity field may also change the intrinsic frequency of the waves. It may also cause a relative Doppler shift between the interfaces. When there is a uniform flow (case 1 of figure 1), there is neither a change in the intrinsic frequency of the waves nor is there a relative Doppler shift between the surface and the interface. However, the bottom ripples are Doppler shifted with respect to the surface and the interface. The dispersion curves for this case has been plotted in figure 2(a) in solid lines. In the dotted lines, we have plotted the dispersion curves without any velocity field. On the vertical axis is the non-dimensionalised frequency ( $\omega^* \equiv \omega/\sqrt{gH}$ ) and on the horizontal axis is the non-dimensional wavenumber  $\alpha \equiv kH$ . The non-dimensionalised velocity is  $U^* \equiv U/\sqrt{gH}$  where  $H = h_u + h_l$ . All the branches of Doppler shifted dispersion curves are simply  $U^*\alpha$  away from the respective branches without the velocity field.

Figure 2(b) shows the dispersion curve for the case when the shear is in the lower layer only (case 2 of figure 1). Thus the Doppler shift component is the same for both external and internal modes, but the only way this differs from case 1 is the presence of shear in lower layer, which has changed the intrinsic frequencies of both external and internal modes.

For the case of shear only in the upper layer (case 3 of figure 1), instead of the pycnocline, the surface undergoes a Doppler shift. Because of shear jump, intrinsic frequencies of both the branches change. It can be seen from the dispersion curve (figure 2(c)) that the branches  $\mathcal{SG}^+$  and  $\mathcal{SG}^-$  are highly non-symmetrical due to presence of the velocity  $U_u$  at the surface. There is a small change in the intrinsic frequency as well, however, it is not evident from the dispersion curves.

In figure 2(d) we have plotted the dispersion curve for the case when both the layers have shear (case 4 of figure 1). For this case, we have assumed the shear to be positive in the upper layer and negative in the lower layer. Thus, the external mode is Doppler shifted positively whereas the internal mode is negatively Doppler shifted.

### 3.1. Shear in the lower layer

Here, we analyse the case when shear is present only in the lower layer and the local velocity at the bottom is zero (case 2 of figure 1). Therefore, the surface modes and the interfacial modes are Doppler shifted by an equal amount with respect to the bottom ripple. Presence of shear will also result in a change in the intrinsic frequencies of the waves. For the case of shear in the lower layer, firstly we investigate the triads formed by two surface modes, i.e.  $\mathcal{SG}^+$  and  $\mathcal{SG}^-$ . We have taken the incident wave  $k_i$  on  $\mathcal{SG}^+$  and the resonant wave  $k_r$  on  $\mathcal{SG}^-$ . Changing the Froude number changes the resonance condition, as is evident from figure 3(a). As mentioned earlier, in the absence of shear, all the Bragg resonance triads having  $k_i$  on the  $\mathcal{SG}^+$  branch will resonate the waves on the  $\mathcal{SG}^-$  branch having  $k_r = k_i$ . This corresponds to the straight line labelled  $Fr = 0.0$  in

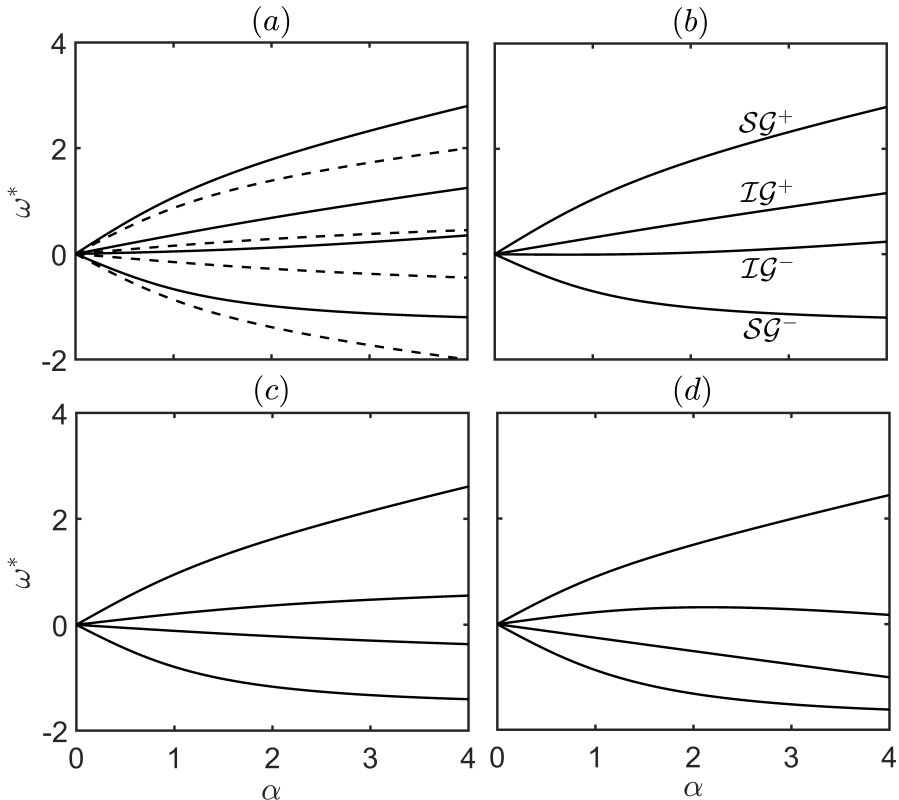


Figure 2: Dispersion relation for various velocity profiles for  $h_u/h_l = 1$ ,  $R = 0.90$  for different velocity profiles (a)  $U_u^* = U_l^* = U_b^* = 0.2$  (b)  $U_u^* = U_l^* = 0.2, U_b^* = 0$  (c)  $U_u^* = 0.2, U_l^* = U_b^* = 0$  (d)  $U_u^* = 0.2, U_l^* = -0.2, U_b^* = 0.2$ .  $\mathcal{SG}^\pm$  denotes surface or external mode,  $\mathcal{IG}^\pm$  denotes interfacial or internal mode, and the + and - signs respectively imply the direction of propagation.

figure 3(a). Increasing the  $Fr$  ( $\equiv U_u/\sqrt{gH}$ ) will mean that the surface will be positively Doppler shifted with respect to the bottom ripples. For any given positive velocity, at some value of  $k$ , the dispersion curve  $\mathcal{SG}^-$  is bound to cross the  $k$ -axis; see figure 3(b). However, while plotting, we have kept the values of  $k$  restricted because for higher values of  $k$ , even though the resonance condition is satisfied, the rate of energy exchange falls off because the waves are unable to ‘feel’ the bottom. We see that for  $Fr = 0.2$ , the  $\mathcal{SG}^-$  branch shifts upwards. This is naturally reflected in the change in the resonance condition in the figure 3(b), in which we have plotted the two branches of the dispersion relation<sup>†</sup>. If  $Fr$  is further increased, then for a given  $k_i$  on  $\mathcal{SG}^+$ , there can be up to 3 values of  $k_r$  on  $\mathcal{SG}^+$  which would form the triad. This is the reason that for  $Fr = 0.6$  curve in figure 3, for a single  $k_i H$ , there exists 3 values of  $k_r H$  for which resonance condition is met. Two of these triads will be formed if the bottom’s wavenumber is  $k_b = k_i + k_r$  (shown by the solid line). However, the third  $k_r$  would lie on the part of  $\mathcal{SG}^-$  for which  $\omega > 0$  and for such a triad (shown in broken lines in figure 3(a) for  $Fr = 0.6$ ), the bottom’s wavenumber would be  $k_r - k_i$ . In the figure 3(b) we have also plotted the change in the

<sup>†</sup> The dispersion relation is a fourth order polynomial in  $\omega$  but we have plotted only two branches on which the resonance is being studied, i.e.  $\mathcal{SG}^+$  and  $\mathcal{SG}^-$  in this case.



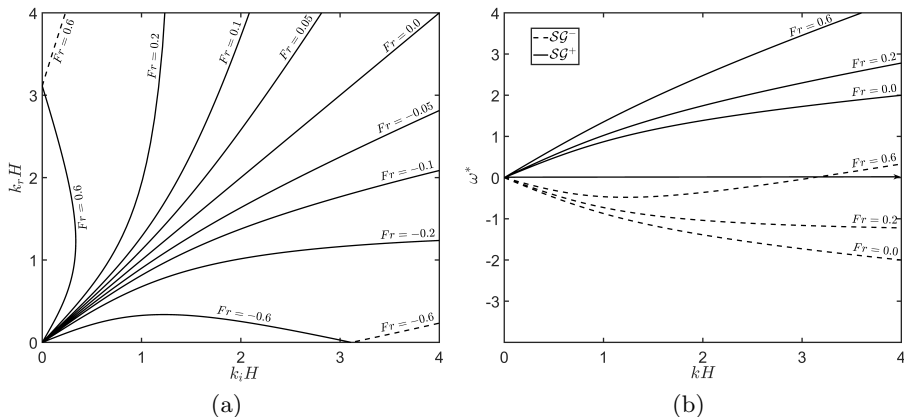


Figure 3: (a) Different combinations of  $k_r$  on  $SG^-$  such that  $k_i$  is on  $SG^+$  for various values of  $Fr \equiv U_u/\sqrt{gH}$  for the case of shear in lower layer.  $R = 0.95$ ,  $h_u/h_l = 1/3$ . For solid lines,  $k_b = k_i + k_r$  but for dashed lines,  $k_b = |k_i - k_r|$ . (b) Dispersion relations for the same case for three values of  $Fr$ . Here solid lines represent  $SG^+$  modes and dashed lines represent  $SG^-$ .

dispersion curves of  $SG^-$  and  $SG^+$  for  $Fr = (0, 0.2, 0.6)$  for  $kH < 4$ . It can be seen that within this window of  $kH$ , for a given  $\omega_i$  on  $SG^+$ , there can be only one  $k_i$  (lines parallel to k-axis i.e.  $\omega = \pm\omega_0$  intersects any given  $SG^+$  at exactly one point). But for a given  $|\omega_r|$  on  $SG^-$ , for  $Fr = 0.6$ , there can be three values of  $k_r$  satisfying the dispersion relation, two values are negative and one positive (lines parallel to k-axis i.e.  $\omega = \pm\omega_0$  may intersect any given  $SG^-$  at either one point or at three points).

Although we have discussed the modification in the resonance condition for a positive  $Fr$ , a very similar thing happens for a negative  $Fr$ . In figure 3, whereas for a positive  $Fr$ , there may exist up to three  $k_r$  on  $SG^-$  for a given  $k_i$  on  $SG^+$ , for a negative  $Fr$  (see  $Fr = 0.6$ ), three different  $k_i$  on  $SG^+$  may resonate the same wavenumber  $k_r$  on  $SG^-$  (see,  $Fr = -0.6$ ). Because the dispersion curves in question, i.e.  $SG^+$  and  $SG^-$  are symmetric for  $Fr = 0$ , the symmetry is also maintained for a positive and a negative  $Fr$ .

It might be noticed that the value of  $Fr$  needed for any appreciable change in the resonance condition varies from moderate to large. The reason for this is that for surface gravity waves, the intrinsic frequency is quite large and to Doppler shift the intrinsic frequency, a local velocity of similar magnitude is needed. For an example, to get three possible resonant waves having  $k_r H < 4$  for a given  $k_i H$ , a Froude number of approximately 0.5 is needed. However, to Doppler shift the interfacial gravity waves on the pycnocline, a significantly lesser value of the Froude number is sufficient because the intrinsic phase speeds of the interfacial waves are significantly low.

We move on to the incident/resonant wave pairs formed by two interfacial modes, i.e. by the waves on  $IG^+$  and  $IG^-$  for the case of shear in the upper layer (case 3). The pycnocline is not only Doppler shifted with respect to the bottom, but it also has a discontinuity in shear across it. This signifies the presence of vorticity-gravity waves at the pycnocline and a significant change in the intrinsic frequency as well. A figure similar to the previous case showing combinations of  $k_i$  (on  $IG^+$ ) and  $k_r$  (on  $IG^-$ ) has been plotted in the figure 4(a) restricting the non-dimensionalised wavenumber to 5. Naturally, at  $Fr = 0$ , the resonance condition is symmetric but the resonance condition changes greatly even for a small amount of mean flow. As we increase the  $Fr$ , for a small

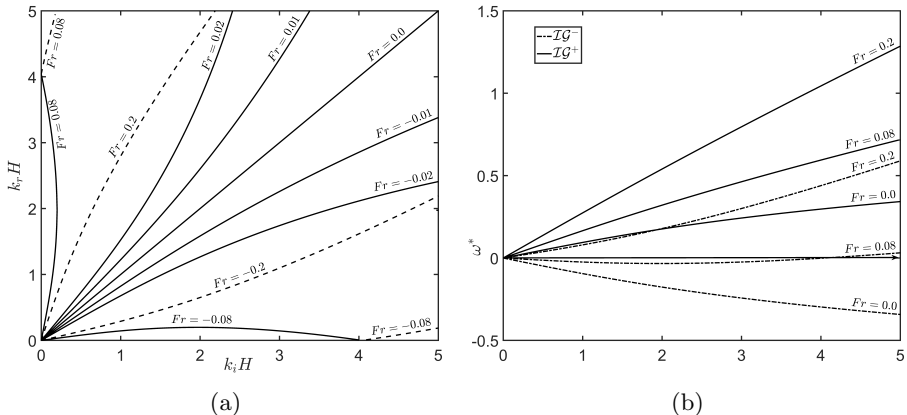


Figure 4: (a) Different combinations of  $k_r$  on  $\mathcal{IG}^-$  such that  $k_i$  is on  $\mathcal{IG}^+$  for various values of  $Fr$  for the case of shear in lower layer.  $R = 0.95$ ,  $h_u/h_l = 1/3$ . For solid lines,  $k_b = k_i + k_r$  but for dashed lines,  $k_b = |k_i - k_r|$ . (b) Dispersion relations for the same case for three values of  $Fr$ . Here solid lines represent  $\mathcal{IG}^+$  modes and dashed lines represent  $\mathcal{IG}^-$ .

$k_i$  on  $\mathcal{IG}^+$ , the resonance condition is met by a larger  $k_r$  on  $\mathcal{IG}^-$  (see curves labelled  $Fr = 0.01, 0.02$  of the figure 4(a)). Further increasing the  $Fr$ , again we see existence of three  $k_r$  for a given  $k_i$ , similar to the resonance between  $\mathcal{SG}^+$  and  $\mathcal{SG}^-$  ( $Fr = 0.08$ , figure 4(a,b)). However, if we further keep on increasing the  $Fr$ , then the complete  $\mathcal{IG}^-$  curve will become positive (shown in the figure 4(b),  $Fr = 0.2$ ) and in such a case, only one resonant wave for any given  $k_i$  on  $\mathcal{SG}^-$  will exist (dashed line labelled  $Fr = 0.2$  in figure 4(a)). The dashed line implies that the wavenumber of the bottom ripple for such a triad is  $k_b = k_i - k_r$  unlike the usual case  $k_b = k_i + k_r$  for the solid lines in figure 4. Again, similar to the previous case, the positive and a negative  $Fr$  result in symmetric cases as shown in the figure 4.

The third sub-case for the case of shear in the upper layer is the resonant interaction between surface and interfacial mode having opposite intrinsic frequency. This means that the incident/resonant pair is either  $\mathcal{IG}^+/\mathcal{SG}^-$  or  $\mathcal{IG}^-/\mathcal{SG}^+$ . Without a loss of generality, we will discuss only the  $\mathcal{IG}^+/\mathcal{SG}^-$  pair; see figure 5(a)-(b). The results about the other pair can be obtained in a straightforward manner, simply by changing the sign of  $Fr$  from positive to negative and vice-versa. What matters is that whether the sign of mean flow and that of surface/interfacial waves are in the same direction or the opposite. The positive shear in this particular case will imply that the velocity at the surface/pycnocline is in the direction of the propagation of the interfacial wave  $\mathcal{IG}^+$ . Therefore, increasing the  $Fr$  will lead to an increase in the frequency of  $\mathcal{IG}^+$  but a non-monotonic change in the frequency of the  $\mathcal{SG}^-$  mode, as shown in the figure 5(b). Even a small value of shear, the effect on the speed of  $\mathcal{IG}^+$  is significant but the  $\mathcal{SG}^-$  is relatively less affected. However, for a large value of  $Fr$ , there may exist multiple values of  $k_r$  for a given  $k_i$  as can be seen from the figure 5(a),  $Fr = 0.3, 0.4, 0.5, 0.6$ . The reason is simply a non-monotonic behaviour of frequency of  $\mathcal{SG}^-$  with respect to the wavenumber as can be seen from figure 5(b). For a higher value of  $Fr$ , the frequency of  $\mathcal{SG}^-$  becomes positive and the triads formed by the positive part of  $\mathcal{SG}^-$  are shown in dashed lines in figure 5(a). For these triads, the bottom's wavenumber is  $k_r - k_i$  whereas for triads marked by solid line, the bottom's wavenumber is  $k_r + k_i$ .

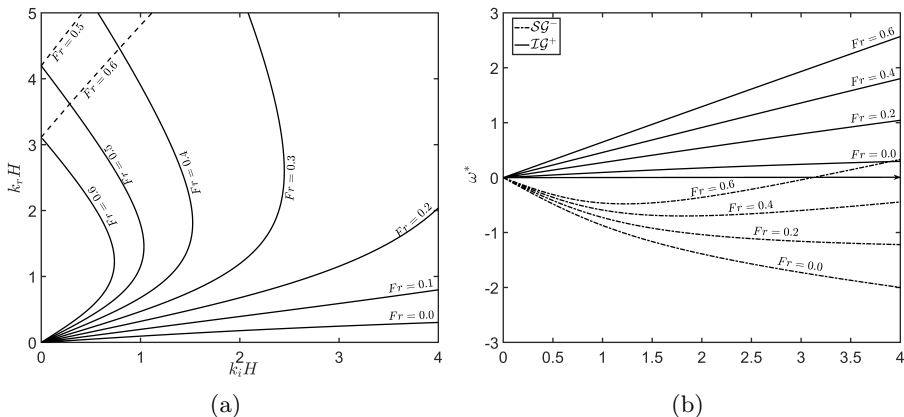


Figure 5: (a) Different combinations of  $k_r$  on  $\mathcal{SG}^-$  such that  $k_i$  is on  $\mathcal{IG}^+$  for various values of positive  $Fr$  for the case of shear in lower layer.  $R = 0.95$ ,  $h_u/h_l = 1/3$ . For solid lines,  $k_b = k_i + k_r$  but for dashed lines,  $k_b = |k_i - k_r|$ . (b) Dispersion relations for the same case for different increasingly positive  $Fr$ . Here solid lines represent  $\mathcal{IG}^+$  modes and dashed lines represent  $\mathcal{SG}^-$ .

If the Froude number is negative (see figure 6(a)-(b)), the frequency of  $\mathcal{SG}^-$  increases monotonically but that of  $\mathcal{IG}^+$  may become non-monotonic; shown in figure 6(b) for the case  $Fr = -0.08$ . Because the frequency of  $\mathcal{SG}^-$  plotted in 6(b) is restricted, not much difference in the dispersion curves is obtained. For a higher  $Fr$ , the frequency changes sign within the chosen limit of  $kH = 4$  and becomes negative ( $Fr = -0.1$ ). For a further increase in the velocity, the frequency becomes completely negative for the  $\mathcal{IG}^-$  ( $Fr = -0.2$ ). This change in the frequency is reflected in the change in the resonance condition and the change can be visualised in the figure 6(a). For  $Fr = -0.01, -0.02, -0.04$ , for a single  $k_r$ , only one  $k_i < 4$  exists but for higher  $Fr$ , a single  $k_r$  maybe resonant by multiple  $k_i$  ( $Fr = -0.08, -0.1$ ). For  $Fr = -0.1$ , the bottom's wavenumber is  $k_i + k_r$  for the solid line part in figure 6(a) and  $k_i - k_r$  for the dashed line part.

Finally, we deal with the case when the incident/resonant modes are in the same direction i.e.  $\mathcal{IG}^+/\mathcal{SG}^+$  or  $\mathcal{IG}^-/\mathcal{SG}^+$ . Again, without a loss of generality, we study only the resonance between  $\mathcal{IG}^+/\mathcal{SG}^+$  modes and in this case, positive  $Fr$  will imply a flow in the same direction of the waves; see figure 7(a)-(b). Because the all the involved waves and the flow are in the same direction, there is no question of sign changing of the frequency of any wave. The frequencies of all the waves increases progressively with increasing  $Fr$  (figure 7(b)). In figure 7(a)-(b), however, we have plotted both the positive  $Fr$  and the negative  $Fr$  having low magnitudes. Increasing the  $Fr$  will mean that for a given  $k_i$ , a higher  $k_r$  will be needed for resonance which can be seen from the figure 7(a)-(b) (positive  $Fr$ ).

For a negative  $Fr$  (see figure 8(a)-(b)), the dispersion relation is plotted in the figure 8(b). For  $Fr = -0.1$ ,  $\mathcal{SG}^+$  is positive throughout but a part of  $\mathcal{IG}^+$  becomes negative. For a higher negative  $Fr$  (say  $-0.3$ ), the  $\mathcal{SG}^+$  still remains positive, but  $\mathcal{IG}^+$  becomes completely negative. For a further negative  $Fr$ , the  $\mathcal{IG}^+$ , remains negative and a part of  $\mathcal{SG}^+$  also becomes negative. The effect on the resonance conditions for the case of small negative  $Fr$  (upto  $-0.25$ ) has been plotted in the figure 7(a) and for higher negative  $Fr$  have been plotted in the figure 8(a).

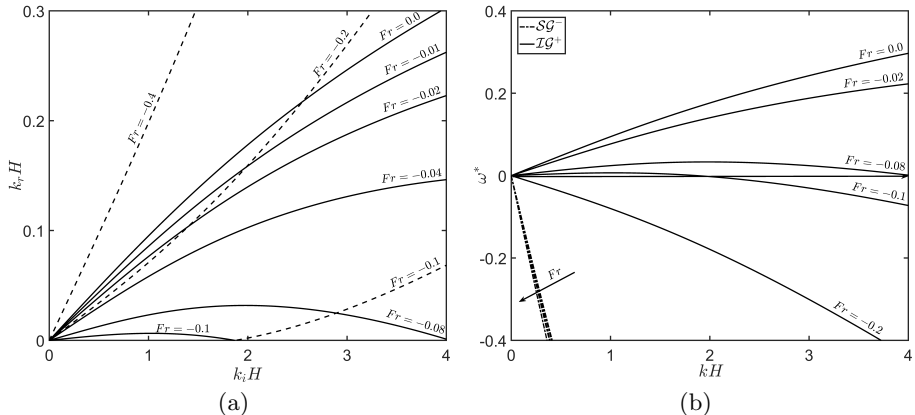


Figure 6: (a) Different combinations of  $k_r$  on  $\mathcal{SG}^-$  such that  $k_i$  is on  $\mathcal{IG}^+$  for various values of negative  $Fr$  for the case of shear in lower layer.  $R = 0.95$ ,  $h_u/h_l = 1/3$ . For solid lines,  $k_b = k_i + k_r$  but for dashed lines,  $k_b = |k_i - k_r|$ . (b) Dispersion relations for the same case for different negative  $Fr$ . Direction of arrows imply increasingly negative  $Fr$ . Here solid lines represent  $\mathcal{IG}^+$  modes and dashed lines represent  $\mathcal{SG}^-$ .

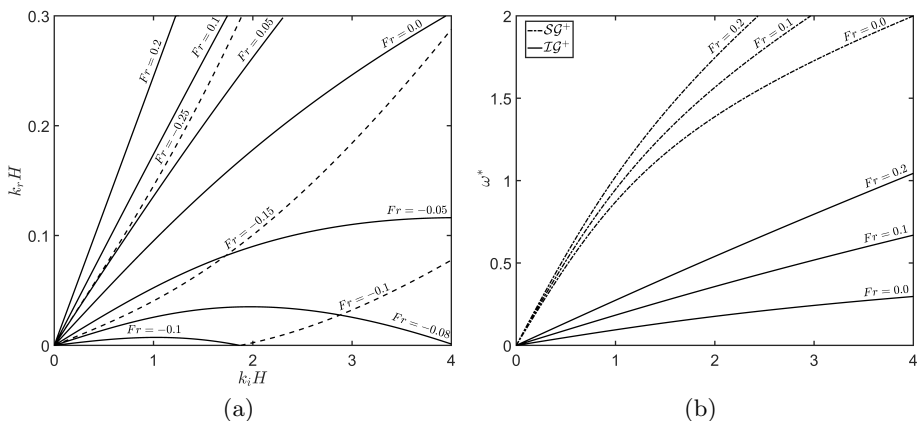


Figure 7: (a) Different combinations of  $k_r$  on  $\mathcal{SG}^+$  such that  $k_i$  is on  $\mathcal{IG}^+$  for various values of positive  $Fr$  and for low values of negative  $Fr$  for the case of shear in lower layer.  $R = 0.95$ ,  $h_u/h_l = 1/3$ . For solid lines,  $k_b = |k_i - k_r|$  but for dashed lines,  $k_b = k_i + k_r$ . (b) Dispersion relation for positive  $Fr$ . Here solid lines represent  $\mathcal{IG}^+$  modes and dashed lines represent  $\mathcal{SG}^+$ .

### 3.2. Shear in the upper layer

As we have mentioned earlier, shear in the upper layer causes a relative Doppler shift of the surface with the pycnocline as well as the bottom ripple. Further, the change in the intrinsic frequencies of the surface modes will be minimal compared to the change in the intrinsic frequencies of the interfacial modes. In §3.1, we have performed a detail study on how the Doppler shift changes the resonance conditions. Here we focus on the case when the intrinsic frequency of the waves get changed, and because the intrinsic frequencies of the interfacial waves are more prone to change, the case of substantial

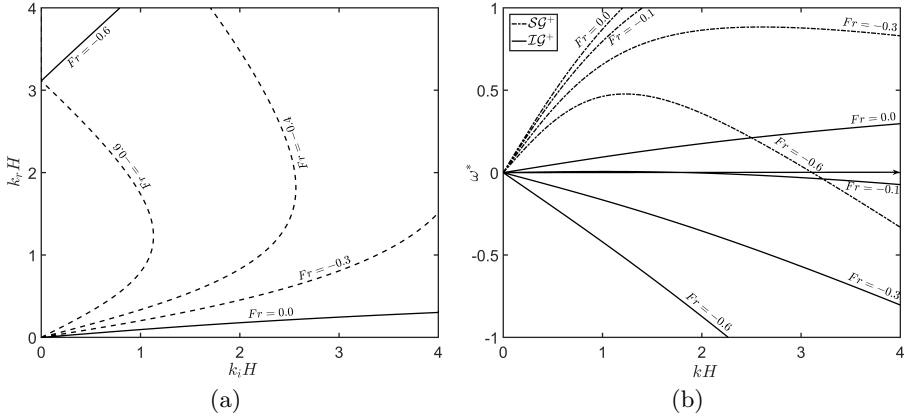


Figure 8: (a) Different combinations of  $k_r$  on  $\mathcal{SG}^+$  such that  $k_i$  is on  $\mathcal{IG}^+$  for various values of positive  $Fr$  and for high values of negative  $Fr$  for the case of shear in lower layer.  $R = 0.95$ ,  $h_u/h_l = 1/3$ . For solid lines,  $k_b = |k_i - k_r|$  but for dashed lines,  $k_b = k_i + k_r$ . (b) Dispersion relation for negative  $Fr$ . Here solid lines represent  $\mathcal{IG}^+$  modes and dashed lines represent  $\mathcal{SG}^+$ .

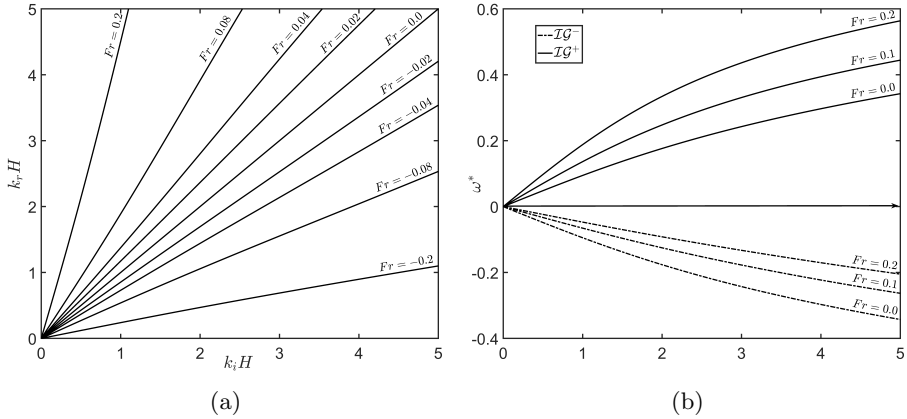


Figure 9: (a) Different combinations of  $k_r$  on  $\mathcal{IG}^-$  such that  $k_i$  is on  $\mathcal{IG}^+$  for various values of  $Fr \equiv U_u/\sqrt{gH}$  for the case of shear in upper layer.  $U_l = U_b = 0$ ,  $R = 0.95$ ,  $h_u/h_l = 1/3$ . (b) Dispersion relations for the same case for three values of  $Fr$ .

interest is the resonant interaction between  $\mathcal{IG}^+$  and  $\mathcal{IG}^-$  modes. Since the shear is only in the upper layer and the pycnocline has no local base velocity, there is no role of Doppler shift. However, when shear in the upper layer is positive ( $Fr > 0$ ), the  $\mathcal{IG}^+$  is sped up but the  $\mathcal{IG}^-$  mode is slowed down (we note that the wave at the interface is a vorticity-gravity wave). Although for the  $Fr = 0$  case, the resonant wave is  $k_r = k_i$ , the conditions change when  $Fr \neq 0$ . For  $Fr > 0$ , we have  $k_r < k_i$ , and for  $Fr < 0$ , we get  $k_r > k_i$ . The change in the resonance condition is shown in the figure 9(a) and the dispersion relation for  $Fr > 0$  has been plotted in the figure 9(b).

## 4. Wave Triad in the presence of a base velocity field

### 4.1. Uniform flow and consequences of shear

Wave triad interaction is energy exchange between waves on the surface and the pycnocline and there is no direct involvement of bottom topography. Therefore, a velocity field with a uniform flow (figure 1 case 1) will Doppler shift the waves on the surface and the pycnocline by the same velocity  $U$  and there won't be any consequences on the resonance condition. To illustrate this, we take three waves having wavenumbers  $(k_1, k_2, k_3)$  and corresponding frequencies  $(\omega_1, \omega_2, \omega_3)$  such that  $k_1 + k_2 - k_3 = 0$  but  $\omega_1 + \omega_2 - \omega_3 \neq 0$ . In the presence of a constant base velocity  $U$ , every frequency  $\omega_i$  ( $i = 1, 2, 3$ ) would be Doppler shifted by an amount  $Uk_i$ . In such a case, however, the intrinsic frequencies of the waves will undergo no change. Therefore, the modified frequency condition would be

$$\begin{aligned} & (\omega_1 + Uk_1) + (\omega_2 + Uk_2) - (\omega_3 + Uk_3) \\ &= \omega_1 + \omega_2 - \omega_3 + U(k_1 + k_2 - k_3) \\ &= \omega_1 + \omega_2 - \omega_3 \\ &\neq 0. \end{aligned}$$

Thus, a mere Doppler shift by the same velocity  $U$  wouldn't change the resonance condition for the wave triad interaction. However, if the surface and the interface were to be Doppler shifted by different amounts, there can be changes in the resonance conditions and naturally the three waves satisfying the resonance condition in the absence of shear might not do so in the presence of a shear. Alternatively, three waves not satisfying a resonance condition might do so in the presence of velocity shear. This can be elucidated using a simple example: let  $k_1 + k_2 - k_3 = 0$  but  $\omega_1 + \omega_2 - \omega_3 \neq 0$ , i.e., the waves do not satisfy the resonant condition in the absence of a base velocity shear. Let us assume that the waves 1 and 2 are at the surface, which now has a base velocity  $U_u$ , while wave 3 is at the interface, which travels with a velocity  $U_l$  (different from  $U_u$  because of shear). Then, the frequency condition reads

$$\begin{aligned} & (\omega'_1 + U_u k_1) + (\omega'_2 + U_u k_2) - (\omega'_3 + U_l k_3) \\ &= \omega'_1 + \omega'_2 - \omega'_3 + U_u(k_1 + k_2) - U_l k_3 \\ &= 0 \quad \text{iff} \quad \omega'_1 + \omega'_2 - \omega'_3 = k_3(U_l - U_u). \end{aligned}$$

The primes in the frequencies denote that the frequencies will get modified due to shear.

### 4.2. Shear in the lower layer

When shear is present only in the lower layer, there is no Doppler shift between the two waves and the only effect of the shear is felt in modifying the intrinsic frequencies of the waves. Although the shear jump is only at the pycnocline, the effect of it at lower wavenumbers would be felt in the surface mode as well. In figure 10(a), we have shown the change in the resonance condition for three interacting waves having  $k_1, k_2$  and  $k_3$  on  $\mathcal{I}\mathcal{G}^-$ ,  $\mathcal{S}\mathcal{G}^-$  and  $\mathcal{I}\mathcal{G}^+$  respectively. The Froude numbers are as follows:  $Fr = (0.0, 0.2, 0.4, 0.6)$ . As the shear is increased in the positive direction, for a given  $k_1$  on  $\mathcal{I}\mathcal{G}^-$ ,  $k_2$  on  $\mathcal{S}\mathcal{G}^-$  decreases but  $k_3$  on  $\mathcal{I}\mathcal{G}^+$  increases. The figure reveals that the change is not as significant as that in the Bragg resonance case even at high values of shear.

### 4.3. Shear in the upper layer

The presence of a shear in the upper layer modifies the flow in two ways. Firstly, there now exists a jump in base shear both at the surface and at the interface, which changes the

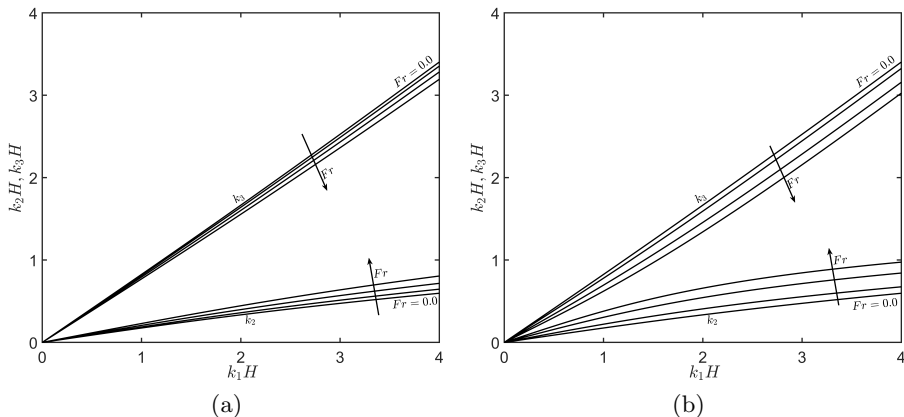


Figure 10: Different combinations of  $k_1$ ,  $k_2$  and  $k_3$  on  $\mathcal{IG}^-$ ,  $\mathcal{SG}^-$ ,  $\mathcal{IG}^+$  respectively forming a resonance triad for (a) shear in bottom layer only.  $U_u^* = U_l^* = (0.0, 0.2, 0.4, 0.6)$ ,  $U_b^* = 0$ ,  $R = 0.95$ ,  $h_u/h_l = 1/3$  (b) shear in top layer only.  $U_u^* = (0.0, 0.2, 0.4, 0.6)$ ,  $U_l^* = U_b^* = 0$ ,  $R = 0.95$ ,  $h_u/h_l = 1/3$ .

intrinsic frequencies of all four modes. Secondly, the presence of a shear automatically means that the local mean velocity at the surface and at the pycnocline are different from each other, which implies a relative Doppler shift between the two. Although such a situation may give rise to shear instabilities, such shear instabilities tend to occur at higher wavenumbers which have very low growth rates. In figure 10(b), we have shown the resonance condition for three interacting waves having  $k_1$ ,  $k_2$  and  $k_3$  respectively on  $\mathcal{IG}^-$ ,  $\mathcal{SG}^-$  and  $\mathcal{IG}^+$ . Yet again, the behaviour is similar to that of previous case but the change in the resonance condition is more prominent here due to the Doppler shifting of the surface and the interface.

## 5. Numerical method

Higher Order Spectral (HOS) method is a highly accurate and efficient numerical method developed by Dommermuth & Yue (1987) for studying wave propagation and wave-topography interaction in a single layered fluid. Among other things, they studied the collision of two wave packets. The method was further expanded to a two-layered density stratified fluid by Alam *et al.* (2009b) to study various cases of Bragg resonance. Although we have derived the evolution equations analytically assuming the resonance conditions are exactly satisfied, the HOS code allows to simulate the near-resonance conditions as well. Furthermore, the study of multiple resonances, which would be a tedious analytical exercise, becomes simpler on using the HOS method. Here our objective is to extend the versatile HOS method to incorporate a piecewise linear velocity field. The base velocity field thus introduced will be continuous but its  $z$ -derivative might be discontinuous at the interfaces, thus giving rise to vorticity gravity waves. In our formulation, we specify the values of the base velocities at  $h = \{0, -h_u, -h_u - h_l\}$  as  $U = \{U_u, U_l, U_b\}$ , using which we get various sub-cases. For  $U_u = U_l = U_b = 0$ , our system will reduce to the system studied in Alam *et al.* (2009b), i.e. having four pure gravity waves. Furthermore, setting  $U_u = U_l = U_b \neq 0$  would lead to gravity waves whose frequencies are simply Doppler shifted with respect to the bottom.

In the HOS method, we solve the evolution of the surface and interface elevations and

velocity potentials associated with them. Rest of the variables in the fluid bulk are solved analytically using the boundary conditions. Since the major part of the computation is limited to the surface and the interface, the HOS method is highly computationally efficient. We proceed similar to what has been described in Alam *et al.* 2009b (with a modification in the sign convention). The continuity equations read

$$\nabla^2 \phi_u = 0 \quad -h_u + \eta_l < z < \eta_u, \quad (5.1a)$$

$$\nabla^2 \phi_u = 0 \quad -h_u - h_l + \eta_b < z < -h_u + \eta_l. \quad (5.1b)$$

The kinematic boundary conditions are as follows:

$$\eta_{u,t} + (U_u + \phi_{u,x})\eta_{u,x} = \phi_{u,z} \quad \text{at } z = \eta_u, \quad (5.2a)$$

$$\eta_{l,t} + (U_l + \phi_{u,x})\eta_{l,x} = \phi_{u,z} \quad \text{at } z = -h_u + \eta_l, \quad (5.2b)$$

$$\eta_{l,t} + (U_l + \phi_{l,x})\eta_{l,x} = \phi_{l,z} \quad \text{at } z = -h_u + \eta_l, \quad (5.2c)$$

$$(U_b + \phi_{l,x})\eta_{b,x} = \phi_{l,z} \quad \text{at } z = -h_u - h_l + \eta_b. \quad (5.2d)$$

Likewise, for the dynamic boundary conditions, we have

$$\phi_{u,t} + \frac{1}{2} (\phi_{u,x}^2 + \phi_{u,z}^2) + U_u \phi_{u,x} - \Omega_u \psi_u + g\eta_u = 0 \quad \text{at } z = \eta_u, \quad (5.3a)$$

$$\rho_u \left[ \phi_{u,t} + \frac{1}{2} (\phi_{u,x}^2 + \phi_{u,z}^2) + U_l \phi_{u,x} - \Omega_u \psi_u + g\eta_l \right] \quad (5.3b)$$

$$-\rho_l \left[ \phi_{l,t} + \frac{1}{2} (\phi_{l,x}^2 + \phi_{l,z}^2) + U_l \phi_{l,x} - \Omega_l \psi + g\eta_l \right] = 0 \quad \text{at } z = -h_u + \eta_l.$$

The governing equation for the potential are simply the Laplace equations, which can't accommodate time evolution in itself. However, there is a time evolution equation for the potentials at the surface and the interface, which are given by the dynamic boundary conditions. We define a surface potential and an interface potential, whose evolution can be tracked using the two dynamic boundary conditions:

$$\phi^S(x, t) \equiv \phi_u(x, \eta_u(x, t), t), \quad (5.4a)$$

$$\phi_1^I(x, t) \equiv \phi_u(x, -h_u + \eta_l(x, t), t), \quad (5.4b)$$

$$\phi_2^I(x, t) \equiv \phi_l(x, -h_u + \eta_l(x, t), t). \quad (5.4c)$$

Further, we define a new potential at the interface using the above defined potentials:

$$\phi^I(x, t) \equiv \phi_1^I(x, t) - R\phi_u^I(x, t). \quad (5.5)$$

Additionally, we define surface and interface streamfunctions

$$\psi^S(x, t) \equiv \psi(x, \eta_u(x, t), t), \quad (5.6a)$$

$$\psi^I(x, t) \equiv \psi(x, -h_u + \eta_l(x, t), t). \quad (5.6b)$$

Using the kinematic and dynamic boundary conditions, we obtain the evolution equations for the surface potential,  $\phi^S$ , the interface potential  $\phi^I$ , the surface elevation,  $\eta_u$  and the



interface elevation,  $\eta_l$ :

$$\eta_{u,t} = -\eta_{u,x}[\phi_{u,x}^S + U_u] + (1 + \eta_{u,x}^2)\phi_{u,z} \quad z = \eta_u, \quad (5.7a)$$

$$\eta_{l,t} = -\eta_{l,x}[\phi_{l,x}^I + U_l] + (1 + \eta_{l,x}^2)\phi_{l,z} \quad z = -h_u + \eta_l, \quad (5.7b)$$

$$\phi_{,t}^S = -g\eta_u - \frac{1}{2}(\phi_{u,x}^S)^2 + \frac{1}{2}(1 + \eta_{u,x}^2)\phi_{u,z}^2 - U_u\phi_{u,x}^S + \Omega_u\psi^S \quad z = \eta_u, \quad (5.7c)$$

$$\begin{aligned} \phi_{,t}^I &= \frac{1}{2}(R(\phi_{1,x}^I)^2 - (\phi_{l,x}^I)^2) + \frac{1}{2}(1 + \eta_{l,x}^2)(\phi_{l,z}^2 - R\phi_{u,z}^2) \\ &\quad - g\eta_l(1 - R) + U_l(R\phi_{u,x}^I - \phi_{l,x}^I) + R\Omega_u\psi_u^I - \Omega_l\psi_l^I \quad z = h_u + \eta_l. \end{aligned} \quad (5.7d)$$

The velocity potential and the streamfunctions are expanded in a perturbation series:

$$\phi_{u/l}(x, z, t) = \sum_{m=1}^M \phi_{u/l}^{(m)}(x, z, t) \quad ; \quad \psi_{u/l}(x, z, t) = \sum_{m=1}^M \psi_{u/l}^{(m)}(x, z, t). \quad (5.8)$$

At every order  $m$ , we further write the velocity potentials as a sum of the basis function (Fourier basis function in this case). Assuming solutions to be periodic in the  $x$ -direction, we express the solutions as a discrete Fourier series<sup>†</sup>. Furthermore, we use the Laplace equations to find out the function form of the solutions, and we finally get

$$\begin{aligned} \phi_u^{(m)} &= \sum_{n=-N}^{N-1} \left[ A_n^{(m)}(t) \frac{\cosh k_n(z + h_u)}{\cosh(k_n h_u)} + B_n^{(m)}(t) \frac{\sinh(k_n h_u)}{\cosh(k_n h_u)} \right] e^{ik_n x}, \quad (5.9) \\ \phi_l^{(m)} &= \sum_{n=-N}^{N-1} \left[ C_n^{(m)}(t) \frac{\cosh k_n(z + h_u + h_l)}{\cosh(k_n h_l)} + D_n^{(m)}(t) \frac{\sinh k_n(z + h_u + h_l)}{\cosh(k_n h_l)} \right] e^{ik_n x}. \end{aligned} \quad (5.10)$$

However, it would not be convenient to directly substitute (5.9) and (5.10) in the boundary conditions to obtain the unknown coefficients because at the surface and the interface,  $z$  will have a dependence on  $x$ . Hence, we would expand the surface and interface potentials as a Taylor Series about the respective mean level, so as to eliminate the implicit  $x$ -dependence of the eigenfunctions:

$$\phi^S(x, t) = \sum_{m=1}^M \phi_u^{(m)}(x, \eta_1, t) = \sum_{m=1}^M \sum_{k=0}^{M-m} \frac{\eta_u^k}{k!} \frac{\partial^k}{\partial z^k} \phi_u^{(m)}(x, z, t) \Big|_{z=0}. \quad (5.11)$$

The above equation can be written as a sequence of Dirichlet boundary conditions at each order  $m$ . Here, the boundary conditions at each order depends on product of the terms which have already been found out at the leading orders, therefore making the problem effectively linear at every order  $m$ . Further details on the derivation of the boundary conditions can be found in Appendix B. We have

$$\phi_u^{(m)}(x, 0, t) = f_1^{(m)}, \quad (5.12)$$

<sup>†</sup> It is necessary to filter out the high wavenumbers by applying a low pass filter due to amplification of round off error at higher wavenumbers; see §3.2.2 of Dommermuth & Yue (1987).

where

$$f_1^{(1)} = \phi^S, \quad (5.13)$$

$$f_1^{(m)} = - \sum_{k=1}^{m-1} \frac{\eta_u^k}{k!} \frac{\partial^k}{\partial z^k} \phi_u^{(m-k)}(x, z, t) \Big|_{z=0}. \quad (5.14)$$

Similarly, for the interface we have a similar sequence of Dirichlet boundary conditions:

$$\Phi^{(m)}(x, -h_1, t) = f_2^{(m)}, \quad (5.15)$$

where

$$f_2^{(1)} = \phi^I, \quad (5.16)$$

$$f_2^{(m)} = - \sum_{k=1}^{m-1} \frac{\eta_l^k}{k!} \frac{\partial^k}{\partial z^k} \Phi^{(m-k)}(x, z, t) \Big|_{z=-h_u}. \quad (5.17)$$

Here we have defined  $\Phi(x, z, t) \equiv \phi_l(x, z, t) - R\phi_u(x, z, t)$ . As for the third boundary condition, we write

$$\varphi_{,z}(x, z, t) = \eta_{l,x} \varphi_{,x}(x, z, t) \quad \text{at } z = -h_u + \eta_l, \quad (5.18)$$

with  $\varphi(x, z, t) \equiv \phi_u(x, z, t) - \phi_l(x, z, t)$ . Using the Taylor expansion of  $\varphi(x, z, t)$  about the mean interface level along with the Laplace equation, we finally get a sequence of Neumann boundary conditions:

$$\varphi_{,z}^{(m)}(x, -h_l, t) = f_3^{(m)}, \quad (5.19)$$

where

$$f_3^{(1)} = 0, \quad (5.20)$$

$$f_3^{(m)} = \sum_{k=1}^{m-1} \frac{\partial}{\partial x} \left[ \frac{\eta_l^k}{k!} \frac{\partial^{k-1}}{\partial z^{k-1}} \varphi_{,x}^{(m-k)}(x, z, t) \Big|_{z=-h_u} \right]. \quad (5.21)$$

Finally, for the bottom boundary condition, we have a similar impenetrability boundary condition:

$$\phi_{l,z}^{(m)}(x, -h_u - h_l, t) = f_4^{(m)}, \quad (5.22)$$

where

$$f_4^{(1)} = U_3 \eta_{b,x}, \quad (5.23)$$

$$f_4^{(m)} = \sum_{k=1}^{m-1} \frac{\partial}{\partial x} \left[ \frac{\eta_b^k}{k!} \frac{\partial^{k-1}}{\partial z^{k-1}} \phi_{l,x}^{(m-k)}(x, z, t) \Big|_{z=-h_u-h_l} \right]. \quad (5.24)$$

Using the four boundary conditions, we obtain the value of unknown coefficients  $A_n$ ,  $B_n$ ,  $C_n$  and  $D_n$  at every order  $m$ . Now we have a full solution of  $\phi_u^{(m)}$  and  $\phi_l^{(m)}$  at the order  $m$ . At the next order  $m+1$ , the functions  $f_1$  to  $f_4$  can be evaluated by using the velocity potentials and their derivatives, which were already found out at the previous order  $m$ . Again the boundary value problem at the order  $m+1$  can be solved, and in this way we can proceed further to obtain  $\phi_u^{(m)}$  and  $\phi_l^{(m)}$  at each order. It is interesting to note here that the all the above four boundary conditions – (5.12), (5.15), (5.19), (5.22) are the same as that in Alam *et al.* (2009b), i.e. without background velocity. Therefore, the function form of the coefficients  $A_n$ ,  $B_n$ ,  $C_n$  and  $D_n$  in terms of the functions  $f_1$  to  $f_4$  remain the same. Using these coefficients, we can find any derivative of the velocity

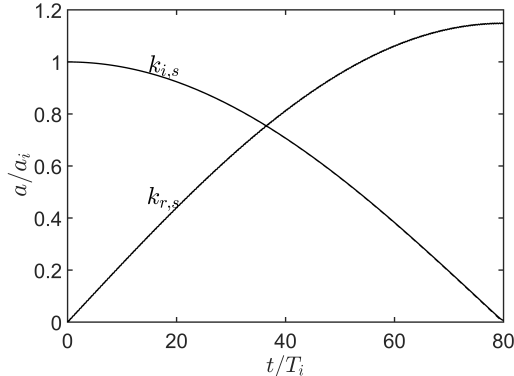


Figure 11: Code Validation for  $R = 0.98$ ,  $k_i H = 0.086$ ,  $k_r H = 0.1140$ ,  $k_b H = 0.2$ ,  $\omega_i^* = 0.0982$ ,  $\omega_r^* = -0.0982$ ,  $U_u^* = 0.1864$ ,  $U_l^* = 0.0083$ ,  $M = 3$ ,  $N = 2048$ ,  $T_i/\Delta T = 512$ . The analytical and numerical solutions are indistinguishable.

potentials at any location. After solving the boundary value problem, we march forward in time using 4-th order Runge-Kutta method. The domain size is chosen to be  $2\pi$  and the number of points in real space equals  $2N + 1$  such that variables are periodic in  $x$ .

### 5.1. Validation

A comprehensive benchmarking of the HOS method for two layers without a velocity field has been performed in Alam *et al.* (2009b). In this paper, we have extended the method to incorporate the velocity field by adding requisite terms. For validation of the code, we have simulated a case of Bragg resonance in which the surface mode interacts with the bottom to generate another surface mode having an intrinsic frequency of the opposite sign. We have compared the solution of the HOS code to the analytically obtained solution. The parameters used are mentioned in the caption of figure 11. It can be seen that the analytical solution and the numerical solution are graphically indistinguishable.

### 5.2. Numerical results

We have simulated a resonance between the waves on the same branch ( $SG^-$ ) of the dispersion curve for the case 2, i.e. shear only in the lower layer. The incident wave has the wavenumber  $k_i H = 0.83$ , while the resonant wave has the wavenumber  $k_r H = 2.27$ . These two waves have the same direction of propagation and have the same frequency of  $\omega^* = -0.4770$ . Because the direction of propagation of the waves is the same, the wavenumber of the bottom is the difference of the wavenumber of the incident and the resonant waves, i.e.  $k_b H = 1.44$ . The velocities are  $U_u^* = 0.5016$ ,  $U_l^* = 0$ ,  $U_b^* = 0$ . Other relevant physical parameters are  $h_u/h_l = 1/3$  and  $R = 0.95$ . The dispersion relation is plotted in figure 12(a) and the corresponding HOS simulation is shown in figure 12(b).

Next, we have studied the effect of shear in upper layer on the Bragg resonance between two oppositely travelling internal modes, i.e.  $IG^+$  and  $IG^-$ . Because the shear is in the upper layer only, there is no Doppler shift of the concerned waves (both on the pycnocline), and the changes are only in the the intrinsic frequencies. In the absence of a base flow, it is known that the resonant wavenumber will be the same as the incident wavenumber. However, we have shown analytically in §4.1 that shear changes the resonance condition. To illustrate this here, we take our incident wave on  $IG^+$  having wavenumber  $k_i H = 0.10$  and frequency  $\omega_i^* = 0.0097$ . The bottom ripple

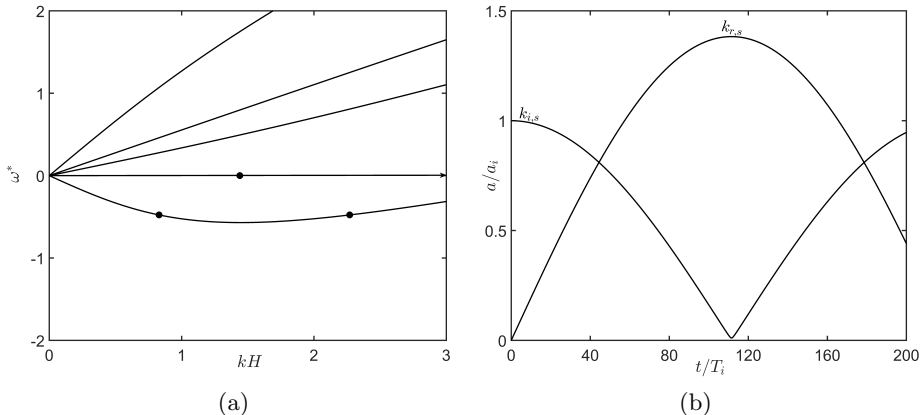


Figure 12: (a) Dispersion relation showing the location of resonant triad. Both the incident and the resonant wave lie on the  $\mathcal{SG}^-$  curve. (b) Numerical simulation using the HOS code:  $a_i = 0.00005H$ ,  $a_b = 0.02H$ ,  $U_u^* = 0.5016$ ,  $U_l^* = U_b^* = 0$ ,  $\omega_i^* = -0.4770$ ,  $R = 0.95$ ,  $k_iH = 0.83$ ,  $k_rH = 2.27$ ,  $k_bH = 1.44$ ,  $h_u/h_l = 1/3$ ,  $M = 3$ ,  $N = 1024$ ,  $T_i/\Delta T = 2048$ .  $T_i$  is the time period of the incident wave.

consists of three different wavenumbers:  $k_{b1}H = 0.19$ ,  $k_{b2}H = 0.20$  and  $k_{b3}H = 0.21$ . Thus, the incident wave will interact with the bottom and may generate three different waves having wavenumbers  $k_{r1}H = 0.09$ ,  $k_{r2}H = 0.10$ ,  $k_{r3}H = 0.11$  and frequencies  $\omega_{r1}H = -0.0088$ ,  $\omega_{r2}H = 0.0097$ ,  $\omega_{r3}H = -0.0107$  respectively. Only one of these wavenumbers may satisfy a resonance condition for a given velocity field and the other wavenumbers will be generated in a ‘near-resonant’ way (Craig 1988). We plot the time evolution of amplitude of all these three wavenumbers in the absence of shear; see figure 13(a). As expected, the maximum growth is only in the wavenumber  $k_{r2}H = 0.10$ . The amplitude plotted is simply the spatial Fourier transform of the interface, and a rapidly changing amplitude corresponding to  $kH = 0.10$  signifies an oppositely travelling wave increasing in amplitude. At about  $t/T_0 \approx 30$ , both the positively and the negatively travelling waves have the same amplitude. We also observe a small growth in the wavenumbers  $kH = 0.09$  and  $kH = 0.11$ . These two wavenumbers do not satisfy the exact resonant condition and hence are generated only near resonantly.

Next, we make the shear negative in the upper layer to yield  $U_u^* = -0.0136$ , while keeping  $U_l^* = U_b^* = 0$ . Due to the velocity field, the incident wave’s frequency gets modified to  $\omega_i^* = 0.0092$ . The frequencies of the three possible resonant waves respectively become  $\omega_{r1}H = -0.0092$ ,  $\omega_{r2}H = -0.0103$  and  $\omega_{r3}H = -0.0103$ . In this case, we observe that the incident wave frequency is equal to  $\omega_{r1}$ , therefore the dominant resonating wavenumber is  $k_{r1}H = 0.09$ . The amplitude evolution has been plotted in see figure 13(b). Wiggles in the plot indicate near-resonant generation of oppositely travelling waves.

Likewise, we make the shear positive in the upper layer to yield  $U_u^* = 0.0123$ , while keeping  $U_l^* = U_b^* = 0$ . The incident wave’s frequency changes to  $\omega_i^* = 0.0102$ . The frequency of the three possible resonant waves become  $\omega_{r1}H = -0.0083$ ,  $\omega_{r2}H = -0.0093$  and  $\omega_{r3}H = -0.0102$ . We observe that  $\omega_i = \omega_{r3}$  and hence, the dominant wavenumber generated is  $k_{r3}H = 0.11$ . This also corroborates with the figure 9, where it can be seen that for a  $k_i$  on  $\mathcal{IG}^+$  mode, increasing the shear results in increase in  $k_r$  on  $\mathcal{IG}^-$  mode. The amplitude evolution has been plotted in see figure 13(c). Again, wiggles indicate near-resonant generation of oppositely travelling waves.

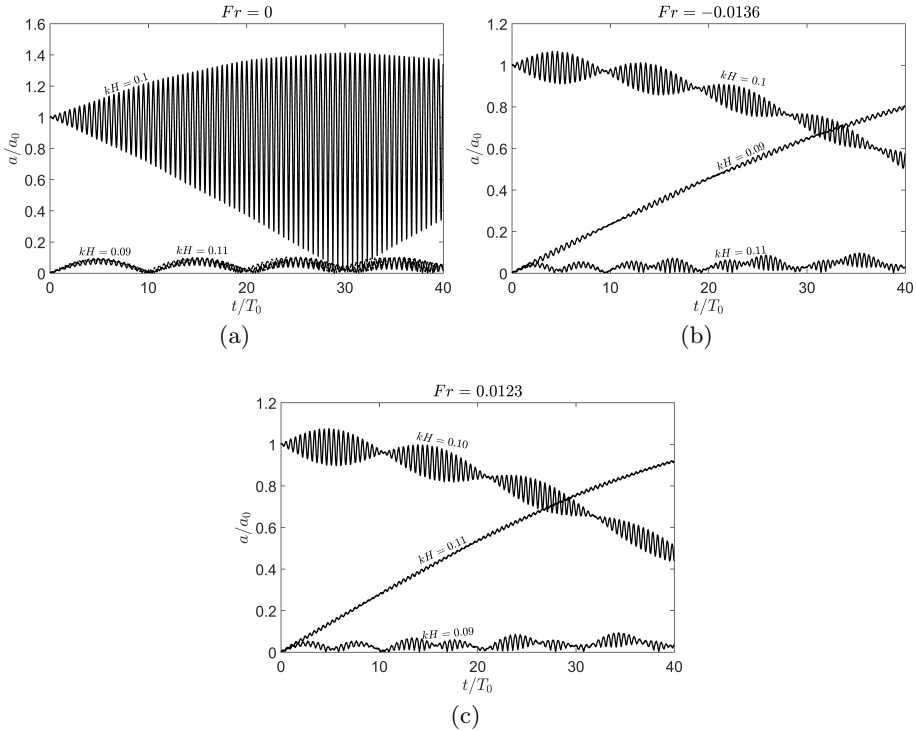


Figure 13: Amplitude vs time plot for different wavenumbers on the interface for  $R = 0.95$ ,  $h_u/h_l = 1/3$ ,  $a_i = 0.00005H_0$ ,  $a_b = 0.05H_0$ , and  $U_l^* = U_b^* = 0$ . (a)  $U_u^* = 0$ , (b)  $U_u^* = -0.0136$ , and (c)  $U_u^* = 0.0123$ . Parameters for the simulation are  $M = 3$ ,  $N = 512$ ,  $T_0/\Delta T = 512$ . Here,  $T_0$  is the time period of the wave  $k_i$  in absence of any background velocity.

## 6. Summary and conclusion

Four wave modes, two at the surface and two at the pycnocline, exist in two-layered density stratified flows. A set of three modes can form a triad and undergo weakly nonlinear interactions when a certain resonance condition is met. A rippled bottom topography, if present, can act as a stationary wave and mediate weakly nonlinear interactions – a process known as ‘Bragg resonance’. The conventional approach towards deriving the standard resonance conditions for weakly nonlinear wave triads, as well as Bragg scattering, fails to incorporate the effect of background velocity, especially of background shear. This is because these approaches are based on the potential flow theory, which dramatically simplifies the problem and allows one to solve for the interfaces only. Since atmospheric and oceanic flows always have background velocity, it is imperative to account for the background flow in studying triads and Bragg resonances. We have taken a step forward in this direction by including piecewise linear velocity profile, while still using the potential flow approximation. Although piecewise linear velocity means piecewise constant shear, and apparently cannot be dealt using potential flow theory, we show that the perturbed flow remains potential, even though the base flow has shear.

On incorporating background velocity, the resonance conditions for wave triads and Bragg scattering get strongly modified. Background velocity influences the resonance

conditions in two ways: (i) by causing unequal Doppler shifts between the surface, pycnocline, and the bottom (at least two of them), and (ii) by changing the intrinsic frequencies of the waves. We have explored various kinds of velocity fields - uniform, constant shear in the lower layer, constant shear in the upper layer, and constant shear in both layers, to form a broad understanding of the effect of background velocity on triads and Bragg resonances. For Bragg resonance, even a uniform velocity field changes the resonance condition. In the absence of background shear, Bragg resonance only occurs when the two wave modes (the third ‘wave’ is the bottom ripple) lie on two distinct branches of the dispersion curve. However with shear (in the lower layer), we show that resonant triads appear even when the two wave modes lie on the same branch of the dispersion curve. In this regard interfacial modes are more susceptible than surface modes; modest Froude numbers are required for causing surface modes on the same branch to resonate; however, small Froude numbers are sufficient to do the same for the interfacial modes.

Using multiple scale analysis along with the Fredholm alternative, we have analytically obtained the equations governing the (slow) time evolution of the amplitudes of the waves forming both classical and Bragg triads up to  $\mathcal{O}(\epsilon^2)$ . The formalism that we have developed has also been added to the Higher Order Spectral (HOS) method, a highly efficient and accurate numerical technique that can incorporate several triads up to any prescribed order of nonlinearity, which traditionally does not include background velocity. Using the ‘modified’ HOS we have numerically studied two problems on Bragg resonance: (i) the case when shear is present in the lower layer and leads to resonance between two wave modes lying on the same branch of the dispersion curve, and (ii) shear in the upper layer, which strongly affects the intrinsic frequencies. In the second case, we consider a bottom ripple consisting of three wavenumbers (chosen close to each other); a given incident wave resonantly generates only one wave resonantly, however two additional waves are generated via near-resonant interactions. Imposing the velocity field leads to change in the standard resonance condition and the wave generated in a near-resonant way may become resonant. This mechanism of near-resonant generation and effect of velocity field on resonance condition has been captured using the modified HOS method.

## Appendix A. Derivation of dynamic boundary condition in the presence of a piecewise linear background shear

The inviscid Navier-Stokes equation within the bulk of a fluid of constant density  $\rho$  is

$$\rho \left[ \mathbf{u}_{,t} + \frac{1}{2} \nabla(\mathbf{u} \cdot \mathbf{u}) - \mathbf{u} \times (\nabla \times \mathbf{u}) \right] = -\nabla p - \nabla(\rho g z). \quad (\text{A } 1)$$

Using the fact that there is no base vorticity generation in the bulk, we have  $\nabla \times \mathbf{u} = \nabla \times \bar{\mathbf{u}} = \Omega \hat{j}$ , where  $\Omega$  is constant for each layer. Besides we use

$$\mathbf{u} \times (\Omega \hat{j}) = \Omega \nabla \psi = \nabla(\Omega \psi). \quad (\text{A } 2)$$

Substituting (A 2) in (A 1) and removing the mean flow part, we are left with

$$\rho \left[ \mathbf{u}'_{,t} + \frac{1}{2} \nabla(\mathbf{u}' \cdot \mathbf{u}') + \nabla(\bar{\mathbf{u}} \cdot \mathbf{u}') - \nabla(\Omega \psi') \right] = -\nabla p' - \nabla(\rho g \eta). \quad (\text{A } 3)$$

Since the perturbed flow is irrotational, we introduce  $\mathbf{u}' = \nabla \phi'$ . Moreover, since density is constant within each layer, we obtain

$$\nabla \left[ \rho \left( \phi'_{,t} + \frac{1}{2} \nabla \phi' \cdot \nabla \phi' + \bar{\mathbf{u}} \cdot \nabla \phi' - \Omega \psi' + g \eta \right) + p' \right] = 0. \quad (\text{A } 4)$$

Since this is true for any arbitrary curve inside the domain, we have on integration

$$\rho \left( \phi'_{,t} + \frac{1}{2} \nabla \phi' \cdot \nabla \phi' + \bar{\mathbf{u}} \cdot \nabla \phi' - \Omega \psi' + g\eta \right) + p' = c, \quad (\text{A } 5)$$

where  $c$  is an arbitrary function of time, which turns out to be zero in order to satisfy the unperturbed far-field condition. Thus, equating the pressure just above and just below the interface  $z = \eta(x, t)$ , at which the base flow velocity is  $\bar{\mathbf{u}} = U\hat{i}$ , we obtain

$$\begin{aligned} \rho_1 \left( \phi'_{1,t} + \frac{1}{2} \nabla \phi'_1 \cdot \nabla \phi'_1 + U\hat{i} \cdot \nabla \phi'_1 - \Omega_1 \psi' + g\eta \right) \\ = \rho_2 \left( \phi'_{2,t} + \frac{1}{2} \nabla \phi'_2 \cdot \nabla \phi'_2 + U\hat{i} \cdot \nabla \phi'_2 - \Omega_2 \psi' + g\eta \right). \end{aligned} \quad (\text{A } 6)$$

Dropping the primes, we get

$$\begin{aligned} \rho_1 \left[ \phi_{1,t} + \frac{1}{2} (\phi_{1,x}^2 + \phi_{1,z}^2) + U\phi_{1,x} - \Omega_1 \psi_1 + g\eta \right] = \\ \rho_2 \left[ \phi_{2,t} + \frac{1}{2} (\phi_{2,x}^2 + \phi_{2,z}^2) + U\phi_{2,x} - \Omega_2 \psi_2 + g\eta \right]. \end{aligned} \quad (\text{A } 7)$$

## Appendix B. Relevant Coefficients

The coefficients  $\mathbf{n}_j$  remains same for the case of wave triad interaction and the case of Bragg resonance. They are simply the null vector of the transpose of the matrix  $\underline{\mathcal{Q}}(k_j, \omega_j)$ . The coefficients of time derivatives of  $\mathcal{O}(\epsilon)$  terms i.e. the vector  $\mathbf{r}_j$  also remains the same both for wave triad interaction and Bragg resonance.

The components of the vector  $\mathbf{r}_j$  are

$$\begin{aligned} r_j(1) &= 1, \\ r_j(2) &= T_j, \\ r_j(3) &= T_j, \\ r_j(4) &= -iQ_j, \\ r_j(5) &= -\frac{i}{k_1} \left[ T_j(\omega_j - k_j U_l) \left( \tanh k_j h_u + \frac{1}{\tanh k_j h_l} \right) + \frac{Q_j}{\cosh k_j h_u} \right], \\ r_j(6) &= 0. \end{aligned}$$

$$\begin{aligned} T_j &= \frac{\cosh(k_j h_u) [(\omega_j - U_u k_j)^2 + (\omega_j - U_u k_j) \Omega_u \tanh(k_j h_u) - g k_j \tanh(k_j h_u)]}{(\omega_j - U_l k_j)(\omega_j - U_u k_j)}, \\ Q_j &= \frac{\Omega_u}{k_j} + \frac{g}{U_u k_j - \omega_j}. \end{aligned}$$

For the case of wave triad interaction the coefficients of  $\mathbf{v}_1$  are as follows:

$$\begin{aligned}
v_1(1) &= -igk_1 \left( \frac{2\Omega_u}{g} + \frac{k_2}{U_u k_2 - \omega_2} + \frac{k_3}{U_u k_3 - \omega_3} \right), \\
v_1(2) &= -ik_1 \left[ \frac{k_2 T_3 Q_2}{\cosh k_2 h_u} + \frac{k_3 T_2 Q_3}{\cosh k_3 h_u} + T_2 T_3 \left( \frac{\omega_2 - U_l k_2}{\tanh k_2 h_u} + \frac{\omega_3 - U_l k_3}{\tanh k_3 h_u} \right) \right], \\
v_1(3) &= -iT_2 T_3 k_1 \left( \frac{k_2 U_l - \omega_2}{\tanh k_2 h_l} + \frac{k_3 U_l - \omega_3}{\tanh k_3 h_l} \right), \\
v_1(4) &= \frac{T_2 (U_l k_2 - \omega_2)}{\cosh k_2 h_l} (k_2 U_u - \omega_2 + k_3 Q_3 \tanh k_3 h_l) \\
&\quad + \frac{T_3 (U_l k_3 - \omega_3)}{\cosh k_3 h_l} (k_3 U_u - \omega_3 + k_2 Q_2 \tanh k_2 h_l) \\
&\quad + (U_u k_3 - \omega_3) k_3 Q_3 \tanh k_2 h_u + (U_u k_2 - \omega_2) k_2 Q_2 \tanh k_2 h_u \\
&\quad - Q_2 Q_3 k_2 k_3 (1 - \tanh k_2 h_u \tanh k_3 h_u) \\
&\quad + \frac{T_2 T_3 (\omega_2 - U_l k_2) (\omega_3 - U_l k_3)}{\cosh k_2 h_u \cosh k_3 h_l} - \Omega_u (k_2 Q_2 + k_3 Q_3), \\
v_1(5) &= T_2 T_3 (R - 1) \left[ (k_3 U_l - \omega_3)^2 + (k_2 U_l - \omega_2)^2 + (k_2 U_l - \omega_2) (k_3 U_l - \omega_3) \right] \\
&\quad - \frac{R k_2 k_3 Q_2 Q_3}{\cosh k_2 h_u \cosh k_3 h_u} + T_2 T_3 (k_2 U_l - \omega_2) \left( R \Omega_u \tanh k_2 h_u + \frac{\Omega_l}{\tanh k_2 h_l} \right) \\
&\quad + T_2 T_3 (k_3 U_l - \omega_3) \left( R \Omega_u \tanh k_3 h_u + \frac{\Omega_l}{\tanh k_3 h_l} \right) \\
&\quad + R k_2 T_3 Q_2 \frac{(k_3 U_l - \omega_3) \tanh k_3 h_u - \Omega_u}{\cosh k_2 h_u} + R k_3 T_2 Q_3 \frac{(k_2 U_l - \omega_2) \tanh k_2 h_u - \Omega_u}{\cosh k_3 h_u} \\
&\quad - T_2 T_3 (k_2 U_l - \omega_2) (k_3 U_l - \omega_3) \left( R \tanh k_2 h_u \tanh k_3 h_u - \frac{1}{\tanh k_2 h_l \tanh k_3 h_u} \right), \\
v_1(6) &= 0.
\end{aligned}$$

Similarly, the terms of the vectors  $\mathbf{v}_2$  and  $\mathbf{v}_3$  can be obtained by changing the indices in a cyclic order, i.e. the substitution  $\{1 \rightarrow 2, 2 \rightarrow 3, 3 \rightarrow 1\}$  in above equations.

For the case of Bragg resonance, we have,

$$\begin{aligned}
v_1(1) &= v_1(2) = v_1(3) = v_1(4) = v_1(5) = 0, \\
v_1(6) &= i \frac{k_1 (\omega_2 - U_l k_2) T_2}{\sinh k_2 h_u}; \\
v_2(1) &= v_2(2) = v_2(3) = v_2(4) = v_2(5) = 0, \\
v_2(6) &= i \frac{k_2 (\omega_1 - U_l k_1) T_1}{\sinh k_1 h_u}.
\end{aligned}$$

The vector  $\mathbf{r}_j$  remains the same as before.

## REFERENCES

- ALAM, M. R., LIU, Y. & YUE, D. K. P. 2009a Bragg resonance of waves in a two-layer fluid propagating over bottom ripples. part I. Perturbation analysis. *J. Fluid Mech.* **624**, 191–224.
- ALAM, M. R., LIU, Y. & YUE, D. K. P. 2009b Bragg resonance of waves in a two-layer fluid propagating over bottom ripples. part II. Numerical simulation. *J. Fluid Mech.* **624**, 225–253.



- BAKER, G. R., MEIRON, D. I. & ORSZAG, S. A. 1982 Generalized vortex methods for free-surface flow problems. *J. Fluid Mech.* **123**, 477–501.
- BALL, F. K. 1964 Energy transfer between external and internal gravity waves. *J. Fluid Mech.* **19**, 465–478.
- CRAIK, A. D. D. 1988 *Wave Interactions and Fluid Flows*. Cambridge University Press.
- DAVIES, AG 1982 The reflection of wave energy by undulations on the seabed. *Dynamics of Atmospheres and Oceans* **6** (4), 207–232.
- DOMMERMUTH, D. G. & YUE, D. K. P. 1987 A high-order spectral method for the study of nonlinear gravity waves. *J. Fluid Mech.* **184**, 267–288.
- DRIVAS, T. D. & WUNSCH, S. 2016 Triad resonance between gravity and vorticity waves in vertical shear. *Ocean Model.* **103**, 87–97.
- ELGAR, STEVE, RAUBENHEIMER, B & HERBERS, THC 2003 Bragg reflection of ocean waves from sandbars. *Geophys. Res. Lett.* **30** (1).
- GUHA, A. & LAWRENCE, G. A. 2014 A wave interaction approach to studying non-modal homogeneous and stratified shear instabilities. *J. Fluid Mech.* **755**, 336–364.
- GUHA, A. & RAJ, R. 2017 Waves and instabilities in stratified shear flows in the absence of gravity. *arXiv preprint arXiv:1709.06627* .
- HARNIK, N., HEIFETZ, E., UMURHAN, O. M. & LOTT, F. 2008 A buoyancy–vorticity wave interaction approach to stratified shear flow. *J. Atmos. Sci.* **65** (8), 2615–2630.
- HEATHERSHAW, AD & DAVIES, AG 1985 Resonant wave reflection by transverse bedforms and its relation to beaches and offshore bars. *Mar. Geol.* **62** (3-4), 321–338.
- HILL, D. F. & FODA, M. A. 1996 Subharmonic resonance of short internal standing waves by progressive surface waves. *J. Fluid Mech.* **321**, 217–233.
- KIRBY, JAMES T 1986 A general wave equation for waves over rippled beds. *Journal of Fluid Mechanics* **162**, 171–186.
- KIRBY, JAMES T 1988 Current effects on resonant reflection of surface water waves by sand bars. *Journal of Fluid Mechanics* **186**, 501–520.
- MEI, CHIANG C 1985 Resonant reflection of surface water waves by periodic sandbars. *Journal of Fluid Mechanics* **152**, 315–335.
- VALLIS, G.K. 2017 *Atmospheric and oceanic fluid dynamics*. Cambridge University Press.
- WEN, F. 1995 Resonant generation of internal waves on the soft sea bed by a surface water wave. *Phys. Fluids* **7**, 1915–1922.